Calculations of the exclusive processes ^{2}H(e, $e'p$)n, ^{3}He(e, $e'p$)^{2}H, and ^{3}He(e, $e'p$)(pn) within a generalized eikonal approximation

C. Ciofi degli Atti and L. P. Kaptari*

Department of Physics, University of Perugia and Istituto Nazionale di Fisica Nucleare, Sezione di Perugia, Via A. Pascoli, I-06123, Italy

(Received 9 July 2004; published 24 February 2005)

The exclusive processes ^{2}H(e, $e'p$)n, ^{3}He(e, $e'p$)^{2}H, and ^{3}He(e, $e'p$)(pn) have been analyzed using realistic few-body wave functions and treating the final state interaction (FSI) within a generalized eikonal approximation (GEA), based on direct calculation of the Feynman diagrams describing the rescattering of the struck nucleon with the nucleons of the $A-1$ system. The approach represents an improvement of the conventional Glauber approach (GA) because it allows one to take into account the effects of the nuclear excitation of the $A-1$ system on the rescattering of the struck nucleon. Using realistic three-body wave functions corresponding to the AV18 interaction, the results of our parameter-free calculations are compared with available experimental data. It is found that in some kinematical conditions FSI effects represent small corrections, whereas in other kinematics conditions they are very large and absolutely necessary to provide a satisfactory agreement between theoretical calculations and experimental data. It is shown that in the kinematics of the experimental data that have been considered, covering the region of missing momentum and energy with $p_m \leqslant 0.6\,\mathrm{GeV}/c$ and $E_m \leqslant 100\,\mathrm{MeV}$ in the perpendicular kinematics, the GA and GEA predictions differ only by less than $\simeq$3–4%.

DOI: 10.1103/PhysRevC.71.024005 PACS number(s): 25.30.−c, 13.40.−f, 21.45.+v, 24.10.Jv

I. INTRODUCTION

One of the main aims nowadays of hadronic physics is the investigation of the limits of validity of the so-called standard model of nuclei, that is, the description of nuclei in terms of the solution of the nonrelativistic Schrödinger equation containing realistic nucleon-nucleon interactions. To this end, exclusive lepton scattering could be very useful, for it might yield relevant information on the nuclear wave function, provided the initial and final states involved in the scattering process are described within a consistent, reliable approach. In the case of *few-body systems*, a consistent treatment of initial and final states is currently possible at low energies (see, e.g., [1,2] and references therein), but at higher energies, when the number of partial waves sharply increases and nucleon-nucleon (NN) interaction becomes highly inelastic, the Schrödinger approach becomes impractical and other methods have to be employed. In the case of *complex nuclei*, additional difficulties arise due to the approximations necessary to solve the many-body problem. In fact, whereas fundamental progress has been made in recent years in the calculation of various properties of light nuclei (see, e.g., [3] and [4] and references therein), much remains to be done for the treatment of the continuum, for which various approximate treatments of the final state cannot be avoided. In this context, it should be stressed that calculations involving few-body systems, where the ground state can be treated exactly, can also be very useful for investigating the limits of validity of various approximate schemes to treat the continuum and their possible extension to complex nuclei.

The aim of this paper is to present the results of a systematic theoretical investigation of the exclusive process $A(e, e'p)B$ off ^{2}H (to be also denoted by D) and ^{3}He, based on a reliable description of the following:

1. initial state correlations (ISC), treated using the state-of-art few-body wave functions [2] corresponding to the AV18 interaction [5], and
2. final state interactions (FSI), treated within a relativistic framework based on calculation of the relevant Feynman diagrams that describe the rescattering of the struck nucleon by the other $A-1$ *spectator* nucleons of the target.

Whereas a correct treatment of ISC in few-body systems is automatically achieved by using realistic wave functions, the treatment of FSI at high energies is still matter of discussion. The approach we are going to use has several nontrivial advantages. It allows one to work within a relativistic framework provided by the use of Feynman diagrams and, moreover, it can be applied, in principle, to the treatment of exclusive $A(e, e'p)B$ processes off complex nuclei as well. It should be stressed, at this point, that the diagrammatic approach we are talking about is not a new one: It has been first formulated in Refs. [6] and [7] (see also Ref. [8]), within a spinless treatment of particle-nucleus scattering, and applied subsequently to various types of high-energy processes with nuclear targets. More recently, the diagrammatic approach has been generalized to the treatment of FSI in exclusive $A(e, e'p)B$ [9–11] and $A(e, e'2p)B$ [12] processes, and a Feynman diagram approach has also been used in Refs. [13,14], [15] to take into account off-shell effects both in inclusive, $A(e, e')X$, and exclusive, $A(e, e'p)B$, processes.

The diagrammatic approach we are referring to is a generalization of the standard Glauber approach (GA) [16] based on the eikonal approximation, so that, following Ref. [12], we will call it the generalized eikonal approximation (GEA).

*On leave from Bogoliubov Laboratory of Theoretical Physics, 141980, JINR, Dubna, Russia.

It is well known that the application of the GA to the treatment of $A(e, e'p)B$ processes requires the following approximations: (i) The *NN* scattering amplitude is obtained within the eikonal approximation; (ii) the nucleons of the spectator system $A-1$ are stationary during the multiple scattering with the struck nucleon (the *frozen approximation*), and (iii) only perpendicular momentum transfer components in the *NN* scattering amplitude are considered. In the GEA the frozen approximation is partly removed by taking into account the excitation energy of the $A-1$ system, which results in a correction term to the standard profile function of the GA, leading to an additional contribution to the longitudinal component of the missing momentum.

In the present paper we apply both the GA and the GEA to the calculation of the processes ^{2}H$(e, e'p)n$, ^{3}He$(e, e'p)^2$H, and ^{3}He$(e, e'p)(np)$, and we compare our results with available experimental data [17–22]. The ^{3}He wave function of the Pisa group [2], corresponding to the AV18 interaction [5], will be used in the calculations. We will not consider, for the time being, meson exchange currents (MEC), Δ-isobar configurations, and similar effects, which have been the object of intensive theoretical studies in $A(e, e'p)B$ processes off both few-body systems (see, e.g., [23,24]) and complex nuclei (see, e.g., [25] and references therein). As in Refs. [9–12], we fully concentrate on the effects of the FSI but we will consider kinematical conditions for which the effects from MEC and Δ excitation effects are expected to be small corrections, and, whenever possible, we will compare our results with those of other authors who include these effects.

The structure of the paper is as follows: In Sec. II the basic formalism of lepton-hadron scattering is briefly illustrated and the main formulas are obtained; in Sec. III the concepts of plane wave impulse approximation and spectral function are recalled; in Sec. IV, the GEA is introduced, the relevant Feynman diagrams that one needs to take into account in the treatment of the full FSI are analyzed, and the problem of the factorization of the lepton-nucleus cross section within the GA and GEA is also discussed; the results of the calculations and their comparison with available experimental data are shown in Sec. V; summary and conclusions are presented in Sec. VI. Some details concerning the formal aspects of our approach are given in Appendixes A and B. Preliminary results of our calculations have been reported in Refs. [26] and [27].

II. BASIC FORMULAS OF $(e, e'p)$ SCATTERING OFF NUCLEI

The one-photon-exchange diagram for the process $A(e, e'p)(A-1)$, where $A-1$ denotes a system of $A-1$ nucleons in a bound or continuum state, is presented in Fig. 1. Shown are the relevant four-momenta in the scattering processes, namely, the electron momenta before and after interaction, $k = (E, \mathbf{k})$ and $k' = (E', \mathbf{k}')$, the momentum of the target nucleus, $P_A = (E_A, \mathbf{P}_A)$, and the momenta of the final proton and the final $A-1$ system, $p_1 = (\sqrt{\mathbf{p}_1{}^2 + M_N^2}, \mathbf{p}_1)$ and $P_{A-1} = \left(\sqrt{\mathbf{P}_{A-1}^2 + (M_{A-1}^f)^2}, \mathbf{P}_{A-1}\right)$, where M_N is the nucleon mass, $M_{A-1}^f = M_{A-1} + E_{A-1}^f$, and E_{A-1}^f is the *intrinsic* excitation energy of the $A-1$ system.

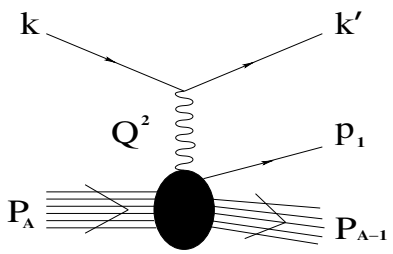

FIG. 1. The one-photon exchange approximation for the process $A(e, e'p)(A-1)$.

Let us briefly recall some useful formulas regarding the process described by the diagram shown in Fig. 1. The differential cross section for the exclusive process has the following form (see, e.g., [28]):

$$\frac{d^6\sigma}{dE'\,d\Omega'\,d^3\mathbf{p}_1} = \sigma_{\rm Mott}\tilde{l}^{\mu\nu}W^A_{\mu\nu}, \tag{1}$$

where $\sigma_{\rm Mott} = 4\alpha^2\,E'^2\cos^2\frac{\theta}{2}/Q^4$ is the Mott cross section, α is the fine-structure constant, $Q^2 = -q^2 = -(k-k')^2 = \mathbf{q}^2 - q_0^2 = 4EE'\sin^2\theta/2$ is the four-momentum transfer, and $\theta \equiv \theta_{\widehat{\mathbf{k}\mathbf{k}'}}$ is the scattering angle. The quantities $\tilde{l}_{\mu\nu}$ and $W^A_{\mu\nu}$ are the reduced leptonic and hadronic tensors, respectively; the former has the well-known standard form [28], whereas the latter can be written as

$$\begin{aligned} W^A_{\mu\nu} = \frac{1}{4\pi M_A}\overline{\sum_{\alpha_A}}\sum_{\alpha_{A-1},\alpha_N}(2\pi)^4\delta^{(4)}(P_A + q - P_{A-1} - p_1) \\ \times\left\langle\alpha_A P_A\middle|\hat{J}^A_\mu(0)\middle|\alpha_N\mathbf{p}_1, \alpha_{A-1}\mathbf{P}_{A-1}E^f_{A-1}\right\rangle \\ \times\left\langle E^f_{A-1}\mathbf{P}_{A-1}\alpha_{A-1}, \mathbf{p}_1\alpha_N\middle|\hat{J}^A_\nu(0)\middle|\alpha_A\mathbf{P}_A\right\rangle, \end{aligned} \tag{2}$$

where α_i denotes the set of discrete quantum numbers of systems A, $A-1$, and N. In Eq. (2) the vector $|\alpha_N\mathbf{p}_1, \alpha_{A-1}\mathbf{P}_{A-1}E^f_{A-1}\rangle$ consists asymptotically of a nucleus $A-1$, with momentum $\mathbf{P}_{A-1}$ and intrinsic excitation energy E^f_{A-1}, and a nucleon with momentum $\mathbf{p}_1$. Two relevant experimentally measurable quantities that characterize the process are the *missing momentum* $\mathbf{p}_m$ (i.e., the momentum of the $A-1$ system) and the *missing energy* E_m defined, respectively, by

$$\begin{aligned} \mathbf{p}_m &= \mathbf{q} - \mathbf{p}_1,\ E_m = \sqrt{P^2_{A-1}} + M_N - M_A \\ &= M_N + M_{A-1} - M_A + E^f_{A-1} = E_{\rm min} + E^f_{A-1}, \end{aligned} \tag{3}$$

where $E_{\rm min} = E_A - E_{A-1} = M_N + M_{A-1} - M_A$, and the (positive) ground-state energies of A and $A-1$ are denoted by E_A and E_{A-1}, respectively. The exclusive cross section can then be written in the well-known form

$$\frac{d^6\sigma}{d\Omega'\,dE'\,d^3\mathbf{p}_m} = \sigma_{\rm Mott}\sum_i V_i W^A_i(\nu, Q^2, \mathbf{p}_m, E_m), \tag{4}$$

where $i \equiv \{L, T, LT, TT\}$, and V_L, V_T, V_{LT}, and V_{TT} are well-known kinematical factors.

The evaluation of the nuclear response functions W_i^A requires knowledge of the nuclear vectors $|\alpha_A \mathbf{P}_A\rangle$ and $|\alpha_N \mathbf{p}_1, \alpha_{A-1}\mathbf{P}_{A-1}E^f_{A-1}\rangle$ and the nuclear current operators $\hat{J}^A_\mu(0)$. Because there is no rigorous quantum field theory to describe, from first principles, a many-body hadronic system, one is forced to adhere to various approximations. Whereas at relatively low energies a consistent nonrelativistic treatment of the electrodisintegration of two- and three-body systems can be pursued, with increasing energy the treatment of the three-body final state requires proper approximations. In the present paper we describe the two- and three-body ground states in terms of realistic wave functions generated by modern two-body interactions [2], and we treat the final state interaction by a diagrammatic approach of the elastic rescattering of the struck nucleon with the nucleons of the $A-1$ system. The relevant diagrams that, within such an approximation, replace the one-photon-exchange diagram of Fig. 1, are shown in Fig. 2: the first one represents the *plane wave impulse approximation* (PWIA); the others show the final state rescattering (FSI).

Although the PWIA appears to have a limited range of validity, it is useful to analyze its predictions, since, within such an approximation, the cross section is directly related to a quantity, the *spectral function*, which, in the case of few-body systems, can be calculated with a high degree of accuracy (see [29–32]). The relevant point here is that, provided the FSI of the struck nucleon with the $A-1$ system can be disregarded, the spectral function yields direct information on the nuclear wave function. For this reason, we will present our results obtained within two distinct approaches:

1. the *PWIA* [Fig. 2(a)], when the struck proton is described by a plane wave, whereas the $A-1$ system in the final state, with momentum P_{A-1}, represents the bound or continuum state solutions of the Schrödinger equation with the same potential used to obtain the A-body wave function. (Note that some authors call the PWIA the state in which *all* particles in the continuum are described by plane waves.)
2. the *full FSI approach* [Figs. 2(b) and 2(c)], when the $A-1$ system (in the ground or continuum states) is still described by the exact solution of the Schrödinger equation, but the interaction of the struck nucleon with the $A-1$ nucleons is treated by evaluating the Feynman diagrams of Fig. 2, in either the GA or the GEA approximations.

III. THE PLANE WAVE IMPULSE APPROXIMATION AND THE NUCLEAR SPECTRAL FUNCTION

The main merit of the PWIA is that it allows one to express the *nuclear* response functions W_i^A in terms of the *nucleon* response functions, which are very well known from $e-N$ experiments. In fact, by expressing the hadronic tensor for the nucleus A [Eq. (2)] in terms of the hadronic tensor for the nucleon N,

$$W^N_{\mu\nu} = \frac{1}{4\pi M_N}\overline{\sum_{\alpha_N}}\sum_{\alpha'_N}(2\pi)^4\delta^{(4)}(p+q-p_1) \times \langle \alpha_N \mathbf{p}_1 | \hat{J}^N_\mu(0) | \alpha'_N \mathbf{p}'_1\rangle\langle \alpha'_N \mathbf{p}'_1 | \hat{J}^N_\nu(0) | \alpha_N \mathbf{p}_1\rangle, \quad (5)$$

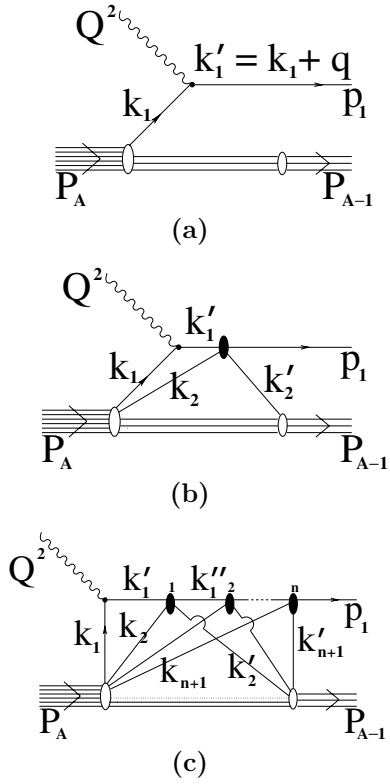

FIG. 2. Feynman diagrams for the process $A(e,e'p)(A-1)$. (a) describes the plane wave impulse approximation (PWIA); (b) the single rescattering; and (c) the full $A-1$ rescattering. The four-momenta of particle i before and after rescattering are denoted by k_i, k'_i, k''_i, etc., respectively. The black ovals denote the elastic nucleon-nucleon scattering matrix.

the cross section assumes the following form (see, e.g., Refs [33–35]):

$$\frac{d^6\sigma}{dE'\,d\Omega'\,d\mathbf{p}_m} = K(Q^2, x, \mathbf{p}_m)\,\sigma^{eN}(\bar{Q}^2, \mathbf{p}_m)P_A(|\mathbf{k}_1|, E), \quad (6)$$

where $\bar{Q}^2 = \mathbf{q}^2 - \bar{q}_0^2$ $(\bar{q}_0 = q_0 + M_A - \sqrt{(\mathbf{k}_1^2 + (M^f_{A-1})^2} - \sqrt{\mathbf{k}_1{}^2 + M_N^2})$, and $K(Q^2, x, \mathbf{p})$ is a kinematical factor. In Eq. (6), $\sigma^{eN}(\bar{Q}^2, \mathbf{p}_m)$ is the cross section describing electron scattering by an off-shell nucleon, $x = Q^2/2M_N q_0$ is the Bjorken scaling variable, $\mathbf{k}_1 = -\mathbf{p}_m$ is the nucleon momentum before interaction, $E \equiv E_{\rm mis} = E_{\rm min} + E^f_{A-1}$ is the *removal energy*, and $P(|\mathbf{k}_1|, E)$ is the nucleon spectral function, which can be written as follows:

$$P(|\mathbf{k}_1|, E) = \frac{1}{(2\pi)^3}\frac{1}{2J_A+1}\sum_f \sum_{\mathcal{M}_A, \mathcal{M}_{A-1}, \sigma_N} \times \left|\langle \alpha_A \mathbf{P}_A | \alpha_N \mathbf{k}_1, \alpha_{A-1}\mathbf{P}_{A-1}E^f_{A-1}\rangle\right|^2 \times \delta\big(E - \big(E^f_{A-1} + E_{\rm min}\big)\big), \quad (7)$$

where $\mathcal{M}_A$, $\mathcal{M}_{A-1}$, and σ_n are the spin projections, and the sum over f includes all possible discrete and continuum states of the $A-1$ system.

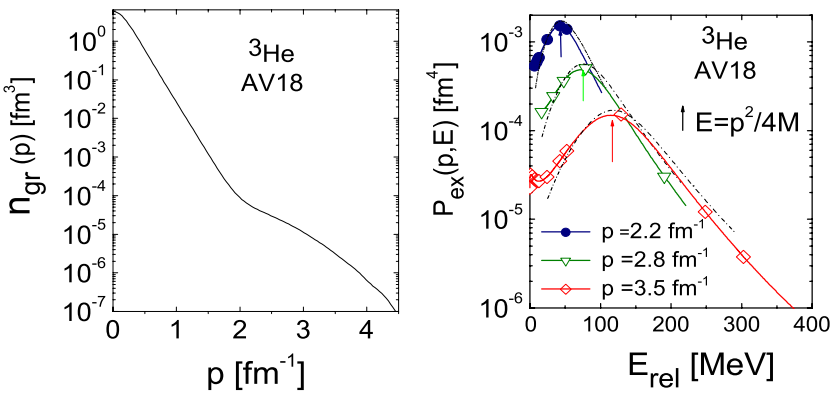

FIG. 3. (Color online) The proton spectral function of ^{3}He [Eq. (9)]. (Left panel) n_{gr} [Eq. (11)] vs $p \equiv |\mathbf{k}_1|$. (Right panel) P_{ex} [Eq. (12)] vs the excitation energy of the two-nucleon system in the continuum $E_{rel} = \mathbf{t}^2/M_N = E_2^f = E - E_{min}$, for various values of $p \equiv |\mathbf{k}_1|$. The dot-dashed curves represent the PWA, when the three particles in the continuum are described by plane waves, whereas the full curves correspond to the PWIA, when the interaction in the spectator proton-neutron pair is taken into account. The arrows indicate the position of the peak ($\sim p^2/4M_N$) predicted by the two-nucleon correlation model for the spectral function [38] (three-body wave function from Ref. [2]; AV18 interaction from [5]).

Whereas the spectral function for the deuteron (D) has a particularly simple form, that is,

$$P_D(|\mathbf{k}_1|, E) = n_D(|\mathbf{k}_1|)\delta(E - \epsilon_D), \tag{8}$$

where ϵ_D is the (positive) binding energy of the deuteron and $n_D(|\mathbf{k_1}|) = (2\pi^2)^{-1}(u_S^2(|\mathbf{k_1}|) + u_D^2(|\mathbf{k_1}|))$ is the nucleon momentum distribution, in the case of $A = 3$, the proton spectral function consists of two parts,

$$P_{\rm He}(|\mathbf{k}_1|, E) = P_{\rm gr}(|\mathbf{k}_1|, E) + P_{\rm ex}(|\mathbf{k}_1|, E), \tag{9}$$

The *ground* part $P_{\rm gr}$ has the following form:

$$P_{\rm gr}(|\mathbf{k}_1|, E) = n_{\rm gr}(|\mathbf{k}_1|)\delta(E - E_{\rm min}), \tag{10}$$

where $E_{\rm min} = |E_3| - |E_2| \approx 5.49$ MeV, and $n_{\rm gr}(|\mathbf{k}_1|)$, which corresponds to the two-body breakup (2bbu) channel $^3{\rm He} \to D + p$, is (hereafter, the projection of the spin of nucleon i will be denoted by s_i)

$$n_{\rm gr}(|\mathbf{k}_1|) = \frac{1}{(2\pi)^3}\frac{1}{2}\sum_{\mathcal{M}_3,\mathcal{M}_2,s_1}\left|\int {\rm e}^{-i\boldsymbol{\rho}\mathbf{k}_1}\chi^\dagger_{\frac{1}{2}s_1} \times \Psi_D^{\mathcal{M}_2\dagger}(\mathbf{r})\Psi_{\rm He}^{\mathcal{M}_3}(\boldsymbol{\rho},\mathbf{r})\,d\boldsymbol{\rho}\,d\mathbf{r}\right|^2. \tag{11}$$

In Eq. (11) $\Psi_{\rm He}^{\mathcal{M}_3}(\boldsymbol{\rho},\mathbf{r})$ is the ^{3}He wave function, $\mathcal{M}_3$ is the projection of the spin of ^{3}He, and $\mathbf{r}$ and $\boldsymbol{\rho}$ are the Jacobi coordinates describing, respectively, the motion of the spectator pair and the motion of the struck (active) nucleon with respect to the c.m. of the pair.

The second, or *excited*, part $P_{\rm ex}$, of $P_{\rm He}(|\mathbf{k}_1|, E)$ corresponds to the three-body breakup (3bbu) channel $^3{\rm He} \to (np) + p$ and can be written as follows:

$$P_{\rm ex}(|\mathbf{k}_1|, E) = \frac{1}{(2\pi)^3}\frac{1}{2}\sum_{\mathcal{M}_3,S_{23},s_1}\int\frac{d^3\mathbf{t}}{(2\pi)^3}\left|\int {\rm e}^{-i\boldsymbol{\rho}\mathbf{k}_1}\chi^\dagger_{\frac{1}{2}s_1}\Psi^{\mathbf{t}\dagger}_{np}(\mathbf{r}) \times \Psi_{\rm He}^{\mathcal{M}_3}(\boldsymbol{\rho},\mathbf{r})d\boldsymbol{\rho}d\mathbf{r}\right|^2\delta\left(E - \frac{\mathbf{t}^2}{M_N} - E_3\right), \tag{12}$$

where $\Psi^{\mathbf{t}}_{np}(\mathbf{r})$ is the two-body continuum wave function characterized by spin projection S_{23} and by the relative momentum $\mathbf{t} = (\mathbf{k}_2 - \mathbf{k}_3)/2$ of the np pair in the continuum. Obviously, for the neutron spectral function, only the excited part (12) contributes.

In Fig. 3 we show the spectral function of ^{3}He obtained using the variational three-body wave function by the Pisa group [2] corresponding to the realistic AV18 potential [5] (see Appendix A). The two-body wave function entering Eq. (12) has been obtained by solving the Schrödinger equation for the continuum using the same AV18 two-nucleon potential. Our results for the spectral function agree with the ones obtained in Ref. [31], where the same three-body wave function has been used. The normalization of the proton spectral function has been fixed to 2 (two protons) and the normalization of the neutron spectral function to 1. In Fig. 3 we also show the results predicted by the plane wave approximation (PWA), which corresponds to the replacement of the continuum interacting $(n - p)$ pair wave function with two plane waves. The left panel of Fig. 3 shows $n_{\rm gr}$ and the right panel $P_{\rm ex}$. It can be seen that (i) $P_{\rm ex}$ exhibits maxima centered approximately at $E_m \sim \mathbf{k}_1{}^2/4M_N$ and (ii) around these values of E_m and $\mathbf{k}_1$ the spectral functions, calculated disregarding the interaction in the NN pair in the continuum (PWA) and taking it into account (PWIA), are almost identical, in agreement with the results obtained long ago [32] with the spectral function corresponding to the Reid soft core interaction [36]. The region centered at $E_m \sim \mathbf{k}_1{}^2/4M_N$ is the so-called two-nucleon correlation region [37], where one of the nucleons of the spectator NN pair is fast, with the other one being basically at rest (for an improved description that takes into account the motion of the third, uncorrelated nucleon, or the $A - 2$ spectator system in case of heavier nuclei, see [38]). Then the fast nucleon becomes strongly correlated with the active nucleon (the proton, in the case of the proton spectral function, or the neutron, in the case of the neutron spectral function) forming a correlated pair that carries most of the nuclear momentum. In this case, it is intuitively expected that the slow nucleon acts as a passive spectator and, consequently, only the interaction in the correlated pair can be relevant for the spectral function. Hence, in this region the calculations including or omitting the interaction in the spectator pair are expected to provide essentially the same results, as confirmed by present and previous calculations of the spectral function

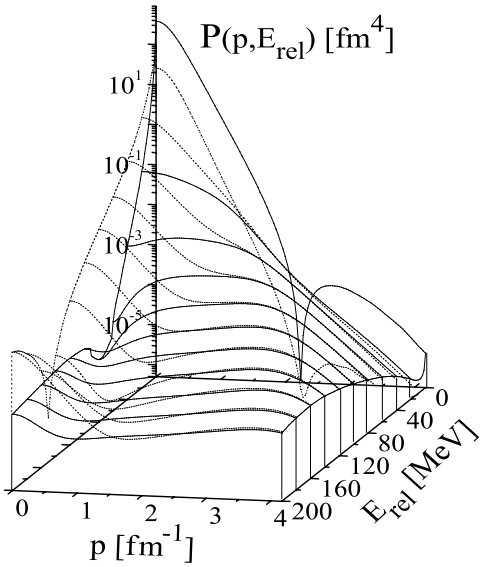

FIG. 4. The neutron spectral function of ^{3}He [Eq. (12)] vs $p \equiv |\mathbf{k}_1|$ and the excitation energy of the two-nucleon system in the continuum $E_{\rm rel} = \mathbf{t}^2/M_N = E_2^f = E - E_{\rm min}$. The dotted curves represent the PWA, when the three particles in the continuum are described by plane waves, whereas the full curves correspond to the PWIA, when the interaction in the spectator proton-proton pair is taken into account (three-body wave function from Ref. [2]; AV18 interaction from [5]).

[26,27,32]. The situation just described is clearly illustrated in Fig. 4, where the three-dimensional neutron spectral function is presented.

The PWIA results suggest that experimental insight about the structure of the nuclear wave function at short distances can be obtained from $A(e, e'p)(A-1)$ processes, provided the PWIA entirely exhausts the reaction mechanism. Unfortunately, we know that in many cases the simplified PWIA mechanism fails to describe the experimental data (see, e.g., a recent discussion in Ref. [39]). However, properly chosen kinematics can still leave room for studying *NN* correlations. It is clear, from Figs. 3 and 4, that such kinematics should be located around the two-nucleon correlation region, in order to exclude the influence of the final state interaction between the spectator nucleons. This requires high values of the missing energy and momentum of the active nucleon (see Fig. 4). Another important condition is that the range of $|\mathbf{q}|$ and q_0 should not be too far from the quasi-elastic peak, where $x \simeq 1$. In this case the corrections from the off-mass shell effects and meson production are minimized, and only the final state interaction of the hit nucleon with the spectators becomes relevant. However, it should always be kept in mind that if a region exists where the interaction *in* the spectator pair (the $A-1$ system in case of complex nuclei) can be neglected, this is no guarantee that the interaction of the struck nucleon *with* the nucleons of the spectator pair (the $A-1$ system) can be neglected as well. It is clear therefore that one has to go beyond the PWIA, which is precisely the aim of the present paper. The effects of the full FSI on the process ^{3}He$(e, e'2p)n$, treating the FSI within the GA have been recently investigated, [40]. In the present paper we will investigate the same topic in the $A(e, e'p)X$ process off ^{2}H and ^{3}He within both the GA and the GEA.

IV. THE FULL FINAL STATE INTERACTION WITHIN THE GENERALIZED EIKONAL APPROXIMATION

Let us consider the interaction of the incoming virtual photon γ^* with a bound nucleon (the active nucleon) of low virtuality ($p^2 \sim M_N^2$) at a kinematics not very different from the quasi-elastic one (i.e., corresponding to $x \sim 1$). In quasi-elastic kinematics, the virtuality of the struck nucleon after γ^* absorption is also rather low and, provided $\mathbf{p}_1$ is sufficiently high, nucleon rescattering with the "spectator" $A-1$ can be described to a large extent in terms of multiple elastic scattering processes in the forward direction (in the system of reference where the target nucleon is at rest). These rescattering processes are diagrammatically depicted in Fig. 2, where, as in the rest of this paper, the internal and intermediate state momenta are denoted by k_i's and the final state momenta by p_i's. The diagrams essentially describe the process of multiple scattering in the most general case, within the assumption that all intermediate nucleons are on-shell. The low virtuality (before and after γ^* absorption) of the active nucleon, coupled with the forward propagation, allows one to simplify the description of the final state interaction, which can be treated within the eikonal approximation. Before illustrating in detail the approach we have used to treat FSI in $(e, e'p)$ reactions, we discuss an important related issue (see also [41]), namely, the validity of the factorization approximation. This approximation is frequently used in calculations at high Q^2 and consists in factorizing the $(e, e'p)$ cross section into e.m. and nuclear parts, despite the fact that factorization, holding exactly in PWIA, is violated when FSI is taken into account. In the next section the factorization approximation will be discussed within the GA and the GEA.

A. The FSI in $A(e, e'p)B$ processes within a diagrammatic approach

Most of the problems one faces when trying to develop a fully covariant treatment of FSI arise because of the hadrons' spins. Therefore, let us rewrite the hadronic tensor [Eq. (2)] in the following, fully equivalent form, which however exhibits explicitly the dependence upon the spin quantum numbers:

$$W^A_{\mu\nu} = \frac{1}{4\pi M_A} \overline{\sum_{\alpha_A}} \sum_{\alpha_{A-1}, s_1} T^\dagger_\mu(\mathcal{M}_A, \mathcal{M}_{A-1}, s_1) \times T_\nu(\mathcal{M}_A, \mathcal{M}_{A-1}, s_1)(2\pi)^4 \delta^{(4)}(P_A + q - P_{A-1} - p_1), \tag{13}$$

where T_μ is a shorthand notation for the transition matrix element

$$T_\mu(\mathcal{M}_A, \mathcal{M}_{A-1}, s_1) \equiv \left\langle \alpha_{A-1} \mathbf{P}_{A-1} E^f_{A-1}, s_1 \mathbf{p}_1 \middle| \hat{J}^A_\mu(0) \middle| \alpha_A \mathbf{P}_A \right\rangle. \tag{14}$$

The basic assumption underlying the eikonal diagrammatic treatment of FSI at high Q^2 is that the transition matrix element

T_μ for a nucleus A can be written in the form

$$T_\mu(\mathcal{M}_A, \mathcal{M}_{A-1}, s_1) = \sum_{n=0}^{A-1} T_\mu^{(n)}(\mathcal{M}_A, \mathcal{M}_{A-1}, s_1), \quad (15)$$

where the superscript (n) corresponds to the order of rescattering of the struck particle with the $A-1$ nucleons (the "spectator" nucleons); namely, $T_\mu^{(0)}$ corresponds to the PWIA (no rescattering), $T_\mu^{(1)}$ to the single rescattering of the struck nucleons with the spectator ones, $T_\mu^{(2)}$ to double rescattering, and so on. Such an approach is expected to be valid either at high energies, when particles propagate mostly in the forward direction along the direction of the three-momentum transfer $\mathbf{q}$, or when the momentum of the struck nucleon $\mathbf{p}_1$ relative to $A-1$ is sufficiently high; in both cases the eikonal approximation could be applied. The calculation of the rescattering part of T_μ in terms of Feynman diagrams appears in principle to be a prohibitive relativistic task owing, as previously stressed, to the treatment of the spin. A relevant simplification occurs if the cross section factorizes into the e.m. and the nuclear parts; in fact, many calculations performed within the eikonal approximation treatment of the FSI simply assume factorization. Let us try to analyze the limits of validity of such an assumption, and to this end let us consider the deuteron. In this case the Feynman diagrams describing rescattering are given in Fig. 5, and the corresponding matrix element is

$$T_\mu(\mathcal{M}_2, s_1, s_2) = T_\mu^{(0)}(\mathcal{M}_2, s_1, s_2) + T_\mu^{(1)}(\mathcal{M}_2, s_1, s_2), \quad (16)$$

where $\mathcal{M}_2$, s_1, and s_2 are the spin projection of the deuteron and of nucleon "1" (the active nucleon) and nucleon "2" (the spectator nucleon) in the final state. Equation (16) obviously states that in the deuteron the interaction between the struck and the spectator nucleon can occur only via single rescattering. The cross section of the process is given by

$$\frac{d^5\sigma}{dE'\,d\Omega'} = \sigma_{\rm Mott} \tilde{l}^{\mu\nu} L^D_{\mu\nu} \frac{d^3p_1}{(2\pi)^3 2E_1} \frac{d^3p_2}{(2\pi)^3 2E_2}, \quad (17)$$

where $E_i = \sqrt{\mathbf{p}_i^2 + M^2}$, and the hadronic tensor is

$$L^D_{\mu\nu} = \frac{1}{2M_D}\frac{1}{3} \sum_{\mathcal{M}_2, s_1, s_2} T^\dagger_\mu(\mathcal{M}_2, s_1, s_2) T_\nu(\mathcal{M}_2, s_1, s_2) \times (2\pi)^4 \delta^{(4)}(P_D + q - p_1 - p_2). \quad (18)$$

Let us now obtain the factorization of the cross section, expressed in terms of the hadronic tensor (18), within a fully covariant approach.

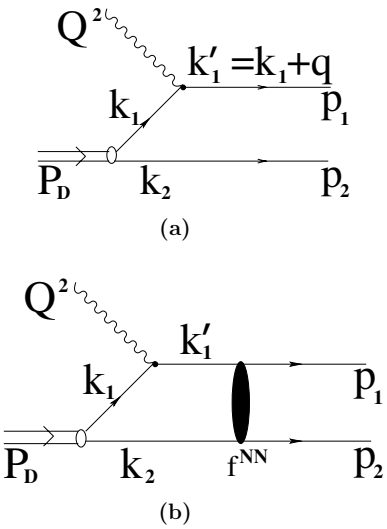

FIG. 5. Feynman diagrams for the process ^{2}H$(e, e'p)n$ representing (a) the PWIA and (b) single rescattering in the final state. f^{NN} denotes the elastic NN scattering amplitude.

1. The PWIA and the factorization of the cross section

The PWIA for the process ^{2}H$(e, e'p)n$ within a covariant Feynman diagram approach has been considered by various authors (see, e.g., [42–44]). The matrix element $T_\mu = T_\mu^{(0)}$ in such a case has the following form:

$$T_\mu^{(0)}(\mathcal{M}_2, s_1, s_2) = \frac{1}{2M_N} \sum_{\tilde{s_1}} J^{eN}_\mu(Q^2, p_1, k_1, \tilde{s}_1, s_1) \times \left[\bar{u}(\mathbf{k}_1, \tilde{s}_1)\Phi_D^{\mathcal{M}_2}(k_1, k_2)(\hat{k}_2 + M_N)v(\mathbf{k}_2, s_2)\right], \quad (19)$$

where

$$J^{eN}_\mu(Q^2, p_1, k_1, \tilde{s}_1, s_1) = \langle \mathbf{p}_1, s_1 | \Gamma^{\gamma^* N}_\mu\left(Q^2, k_1^2\right) | \mathbf{k}_1, \tilde{s}_1 \rangle, \quad (20)$$

$\Gamma^{\gamma^* N}_\mu(Q^2, k_1^2)$ is the e.m. vertex, and $\Phi_D^{\mathcal{M}_2}(k_1, k_2)$ is the covariant deuteron amplitude corresponding to the D $\to (pn)$ vertex. The explicit form of the amplitude $\Phi_D^{\mathcal{M}_2}(k_1, k_2)$ depends on the specific covariant model used to describe the deuteron and could be found elsewhere (see, e.g., [42,43,45]). Here, without loss of generality, we will use the Bethe-Salpeter (BS) formalism according to Refs. [45] and [44].

When Eq. (19) is placed into Eq. (18), the e.m. and nuclear parts get coupled by the summation over the intermediate spins $\tilde{s}_1$ and $\tilde{s}_1{}'$. However, it can be shown (see Appendix B) that the square of the expression in brackets in Eq. (19) after summation over $\mathcal{M}_2$ and s_2 yields a δ function $\delta_{\tilde{s}_1\tilde{s}_1'}$ (i.e., becomes diagonal in $\tilde{s}_1$); this leads to the decoupling between the e.m. and the nuclear parts in Eq. (19), with the resulting hadronic tensor given by

$$L^D_{\mu\nu} = \frac{1}{2M_D}\frac{1}{3} \sum_{\mathcal{M}_2, s_1, s_2} T^\dagger_\mu(\mathcal{M}_2, s_1, s_2) T_\nu(\mathcal{M}_2, s_1, s_2) = 2M_D \left(2E_{\mathbf{p}_1} 2E_{\mathbf{k}_1} L^{eN}_{\mu\nu}(Q^2, p_1, k_1)\right) \times n_D(|\mathbf{k}_1|)(2\pi)^4 \delta^{(4)}(P_D + q - p_1 - p_2). \quad (21)$$

In Eq. (21), n_D is the deuteron momentum distribution given by

$$n_D(|\mathbf{k}_1|) = \frac{1}{3} \sum_{\mathcal{M}_2, \tilde{s}_1, s_2} \left|\left[\bar{u}(\mathbf{k}_1, \tilde{s}_1)\Phi_D^{\mathcal{M}_2}(k_1, k_2) \times (\hat{k}_2 + M_N)v(\mathbf{k}_2, s_2)\right]\right|^2$$

$$= \frac{1}{3}\sum_{\mathcal{M}_2,\tilde{s}_1,s_2} \left|\langle \tilde{s}_1, s_2|\Psi_D^{\mathcal{M}_2}(\mathbf{k_1})\rangle\right|^2$$
$$= \frac{1}{2\pi^2}\left(u_S^2(|\mathbf{k_1}|) + u_D^2(|\mathbf{k_1}|)\right), \quad (22)$$

where the (covariant) deuteron wave function has been cast in a form similar to the nonrelativistic one with the scalar parts of the wave function, $u_L(|\mathbf{k}|)$'s, related to the corresponding vertex functions, $G_L(k_1^2, k_2^2 = M_N^2)$, by a well-known definition [see Eqs. (B8) and (B9)], leading to

$$u_L(|\mathbf{k}|) \sim \sqrt{2M_N}\frac{G_L(|\mathbf{k}|, k_{10} = M_D - E_{\mathbf{k}})}{k^2 - M_N^2}. \quad (23)$$

Placing Eq. (21) in Eq. (17) the well-known factorized form for the cross section is obtained:

$$\frac{d^6\sigma}{dE'\,d\Omega'\,d\mathbf{p}_m} = K(Q^2, x, \mathbf{p}_m)\,\sigma^{eN}(\bar{Q}^2, \mathbf{p}_m) n_D(|\mathbf{k}_1|)) \times \delta\left(q_0 + M_D - E_{\mathbf{k}_1+\mathbf{q}} - E_{\mathbf{k}_i}\right). \quad (24)$$

We reiterate that factorization has been obtained because the sum over s_2 and $\mathcal{M}_2$ in (18) leads to the appearance of a δ function $\delta_{\tilde{s}_1',\tilde{s}_1}$, which means, in turn, that the square of $T_\mu^{(0)}$ becomes diagonal in $\tilde{s}_1$. This particular (exact) result is part of a more general assertion that within the PWIA the nuclear spectral function is always diagonal in spins [35]. Let us now consider FSI; in this case the tensor (18) is off-diagonal in spins and factorization does not occur. However, we will show that under certain kinematical conditions, satisfied to a large extent by the GA and GEA, factorization can be recovered.

2. FSI: single scattering contribution and factorization of the cross section

Let us compute the second diagram of Fig. 5. To this end, we introduce a two-nucleon scattering operator $\hat{T}$ in terms of which the elastic scattering amplitude f^{NN}, describing the elastic scattering of two on-shell nucleons, will be defined as follows

$$f^{NN}_{\tilde{s}_1\tilde{s}_2;s_1,s_2}(\mathbf{p}_1, \mathbf{p}_2; \mathbf{k}_1, \mathbf{k}_2) = \bar{u}(\mathbf{p}_1, s_1)\bar{u}(\mathbf{p}_2, s_2)\,\hat{T} \times u(\mathbf{k}_1, \tilde{s_1})u(\mathbf{k}_2, \tilde{s_2}), \quad (25)$$

which is obviously the free NN scattering amplitude; for a bound nucleon one has in principle to consider off-shell effects but in the GEA no virtuality is considered; this could be done for example by the approach of Ref. [14], by introducing cutoff form factors in the corresponding nucleon lines, which formally leads to two Feynman diagrams with different "nucleonic" masses. In the presence of FSI, the transition matrix element is

$$T_\mu(\mathcal{M}_2, s_1, s_2) = T_\mu^{(0)}(\mathcal{M}_2, s_1, s_2) + T_\mu^{(1)}(\mathcal{M}_2, s_1, s_2) \quad (26)$$

with $T_\mu^{(0)}$ given again by Eq. (19), and $T_\mu^{(1)}$ is given by the following form (note that henceforth we always have $\mathbf{k}_1 = -\mathbf{k}_2$):

$$T_\mu^{(1)}(\mathcal{M}_2, s_1, s_2) = \frac{1}{2M_N}\sum_{\tilde{s}_1\tilde{s}_1'\tilde{s}_2}\int\frac{d^4k_2}{i(2\pi)^4} \times \frac{f^{NN}_{\tilde{s}_1'\tilde{s}_2;s_1,s_2}(\mathbf{p}_1, \mathbf{p}_2, \mathbf{k}_1', \mathbf{k}_2)}{k_1'^2 - M_N^2 + i\varepsilon} \times \left[\bar{u}(\mathbf{k}_1', \tilde{s}_1')\Gamma_\mu^{\gamma^*N}(Q^2, k_1'^2)u(\mathbf{k}_1, \tilde{s}_1)\right] \times \left[\bar{u}(\mathbf{k}_1, \tilde{s}_1)\Phi_D^{\mathcal{M}_2}(k_1, k_2)v(\mathbf{k}_2, \tilde{s}_2)\right]. \quad (27)$$

The full matrix element will therefore be

$$T_\mu(\mathcal{M}_2, s_1, s_2) = \frac{1}{2M_N}\sum_{\tilde{s}_1} J_\mu^{eN}(Q^2, \mathbf{p}_1, \mathbf{p}_m, \tilde{s}_1, s_1) \times \left[\bar{u}(\mathbf{k}_1, \tilde{s}_1)\Phi_D^{\mathcal{M}_2}(k_1, k_2)(\hat{k}_2 + M_N)v(\mathbf{k}_2, s_2)\right] + \frac{1}{2M_N}\sum_{\tilde{s}_1\tilde{s}_1'\tilde{s}_2}\int\frac{d^4k_2}{i(2\pi)^4}\frac{f^{NN}_{\tilde{s}_1'\tilde{s}_2;s_1,s_2}(\mathbf{p}_1, \mathbf{p}_2, \mathbf{k}_1', \mathbf{k}_2)}{k_1'^2 - M_N^2 + i\varepsilon} \times \left[\bar{u}(\mathbf{k}_1', \tilde{s}_1')\Gamma_\mu^{\gamma^*N}(Q^2, k_1'^2)u(\mathbf{k}_1, \tilde{s}_1)\right] \times \left[\bar{u}(\mathbf{k}_1, \tilde{s}_1)\Phi_D^{\mathcal{M}_2}(k_1, k_2)v(\mathbf{k}_2, \tilde{s}_2)\right]. \quad (28)$$

When Eq. (28) is placed into Eq. (18), the resulting equation is not diagonal in the spin quantum numbers and factorization does not hold. Let us however consider the basic assumptions underlying the eikonal multiple scattering approach:

1. The momentum transfer $\boldsymbol{\kappa}$ in the elastic rescattering is small and mostly transverse, that is,
$$\boldsymbol{\kappa} = \mathbf{p}_1 - \mathbf{k}_1' = \mathbf{k}_2 - \mathbf{p}_2 \simeq \mathbf{k}_{2\perp} - \mathbf{p}_{2\perp} = \boldsymbol{\kappa}_\perp \quad (29)$$
2. The spin-flip part of the NN amplitude is very small, which means that, taking into account the previous assumption, one can write
$$f^{NN}_{\tilde{s}_1'\tilde{s}_2;s_1,s_2}(\mathbf{p}_1, \mathbf{p}_2, \mathbf{k}_1', \mathbf{k}_2) \approx \delta_{\tilde{s}_1',s_1}\delta_{\tilde{s}_2,s_2} f^{NN}(\boldsymbol{\kappa}_\perp), \quad (30)$$
which is realized either at high values of the three-momentum transfer $\mathbf{q}$, or at high values of the momentum $\mathbf{p}_1$ of the struck nucleon relative to the $A-1$ spectator nucleons.

If these conditions are satisfied, Eq. (27) assumes the following form (cf. Appendix B):

$$T_\mu^{(1)}(\mathcal{M}_2, s_1, s_2) \simeq \sum_{\tilde{s}_1} J_\nu^{eN}(Q^2, \mathbf{p}_m, \mathbf{p}_1, \tilde{s}_1, s_1) \times \frac{1}{2M_N}\int\frac{d^4k_2}{i(2\pi)^4}\frac{f^{NN}(\boldsymbol{\kappa}_\perp)}{k_1'^2 - M_N^2 + i\varepsilon} \times \left[\bar{u}(\mathbf{k}_1, \tilde{s}_1)\Phi_D^{\mathcal{M}_2}(k_1, k_2)v(\mathbf{k}_2, s_2)\right] \quad (31)$$

and one can write

$$T_\mu(\mathcal{M}_2, s_1, s_2) \simeq \frac{1}{2M_N}\sum_{\tilde{s}_1} J_\nu^{eN}(Q^2, \mathbf{p}_m, \mathbf{p}_1, \tilde{s}_1, s_1) \times \left\{\left[\bar{u}(\mathbf{k}_1, \tilde{s}_1)\Phi_D^{\mathcal{M}_2}(k_1, k_2)(\hat{k}_2 + M_N)v(\mathbf{k}_2, s_2)\right]\right.$$

$$+\int \frac{d^4k_2}{i(2\pi)^4}\frac{f^{NN}(\boldsymbol{\kappa}_\perp)}{k_1'^2-M_N^2+i\varepsilon}\times\left[\bar{u}(\mathbf{k}_1,\tilde{s}_1)\Phi_D^{\mathcal{M}_2}(k_1,k_2)v(\mathbf{k}_2,s_2)\right]\Bigg\}. \quad (32)$$

It can be seen that $T_\mu^{(0)}$ and $T_\mu^{(1)}$ in Eq. (32) have very similar structures, except that in $T_\mu^{(1)}$ the vector $\mathbf{k}_2$ is now an integration variable, since $\mathbf{k}_2 \neq \mathbf{p}_2$. When Eq. (18) is evaluated, with T_μ given by Eq. (32) and assuming soft *NN* rescattering (low values of $\boldsymbol{\kappa}_\perp$), the main contribution in the integral over $\mathbf{k}_2$ results from the region where $\mathbf{k}_2 \sim \mathbf{p}_2$ and this, in turn, originates again a delta function $\delta_{\tilde{s}_1 s_1}$ (see Appendix B) and the hadronic tensor becomes

$$\begin{aligned}L^D_{\mu\nu} &= \frac{1}{2M_D}\frac{1}{3}\sum_{\mathcal{M}_2,s_1,s_2} T^\dagger_\mu(\mathcal{M}_2,s_1,s_2)\cdot T_\nu(\mathcal{M}_2,s_1,s_2)\\ &\times(2\pi)^4\delta^{(4)}(P_D+q-p_1-p_2)\\ &\simeq \frac{1}{2}\sum_{\tilde{s}_2,s_1}\left[J^{eN\dagger}_\mu(Q^2,\mathbf{p}_m,\mathbf{p}_1,\tilde{s}_2,s_1)\right.\\ &\left.\cdot J^{eN}_\nu(Q^2,\mathbf{p}_m,\mathbf{p}_1,\tilde{s}_2,s_1)\right]\\ &\times\frac{1}{(2M_N)^2}\sum_{\mathcal{M}_2\tilde{s}_1,s_2}\Bigg|\left[\bar{u}(\mathbf{k}_2,\tilde{s}_1)\Phi_D^{\mathcal{M}_2}\right.\\ &\left.\times(k_1,k_2)(\hat{k}_2+M_N)v(\mathbf{k}_2,s_2)\right]_{k_2=p_2}\\ &+\int\frac{d^4k_2}{i(2\pi)^4}\frac{f^{NN}(\boldsymbol{\kappa}_\perp)}{k_1'^2-M_N^2+i\varepsilon}\\ &\times[\bar{u}(\mathbf{k}_2,\tilde{s}_1)\Phi_D^{\mathcal{M}_2}(k_1,k_2)v(\mathbf{k}_2,s_2)]\Bigg|^2\\ &\times(2\pi)^4\delta^{(4)}(P_D+q-p_1-p_2) \quad (33)\end{aligned}$$

and the factorization of the e.m. and the nuclear parts is recovered. Equation (33) could be written in a more familiar form if one integrates over k_{20} by taking into account the pole in the amplitude $\Phi_D^{\mathcal{M}_2}(k_1,k_2)$ ($k_{20}=E_{\mathbf{k}}$) and neglecting the pole from the active propagator, which is located at large values of k_{20} and does not contribute to the integral. Using (22) and (23) one obtains $[\int d^4k/[i(2\pi)^4] \to \int d^3k/[2E_{\mathbf{k}}(2\pi)^3]]$

$$\begin{aligned}L^D_{\mu\nu} &\simeq 2M_D\left[2E_{\mathbf{p}_1}2E_{\mathbf{p}_m}L^N_{\mu\nu}(Q^2,\mathbf{p}_m,\mathbf{p}_1)\right]\\ &\times\sum_{\mathcal{M}_2,s_1,s_2}\Bigg|\left\langle s_1,s_2\middle|\Psi_D^{\mathcal{M}_2}(\mathbf{k}_2)\right\rangle_{k_2=p_2}+\int\frac{d^3k_2}{2E_{\mathbf{k}_2}(2\pi)^3}\\ &\times\frac{f^{NN}(\boldsymbol{\kappa}_\perp)}{k_1'^2-M_N^2+i\varepsilon}\left\langle s_1,s_2\middle|\Psi_D^{\mathcal{M}_2}(\mathbf{k}_2)\right\rangle\Bigg|^2\\ &\times(2\pi)^4\delta^{(4)}(P_D+q-p_1-p_2). \quad (34)\end{aligned}$$

By placing this equation into Eq. (17), one obtains

$$\begin{aligned}\frac{d^6\sigma}{dE'\,d\Omega'\,d\mathbf{p}_m} &= K(Q^2,x,\mathbf{p}_m)\sigma^{eN}(\bar{Q}^2,\mathbf{p}_m)\\ &\times n_D^{\mathrm{FSI}}(\mathbf{p}_m)\delta(q_0+M_D-E_{\mathbf{p}_1+\mathbf{q}}-E_{\mathbf{p}_2}), \quad (35)\end{aligned}$$

where the *distorted momentum distribution* n_D^{FSI} is

$$\begin{aligned}n_D^{\mathrm{FSI}}(\mathbf{p}_m) &= \frac{1}{3}\sum_{\mathcal{M}_2,s_1,s_2}\Bigg|\left\langle s_1,s_2\middle|\Psi_D^{\mathcal{M}_2}(\mathbf{k}_2)\right\rangle_{k_2=p_2}\\ &+\int\frac{d^3k_2}{2E_{\mathbf{k}_2}(2\pi)^3}\frac{f^{NN}(\boldsymbol{\kappa}_\perp)}{k_1'^2-M_N^2+i\varepsilon}\left\langle s_1,s_2\middle|\Psi_D^{\mathcal{M}_2}(\mathbf{p}_m)\right\rangle\Bigg|^2\\ &= \frac{1}{3}\sum_{\mathcal{M}_2,s_1,s_2}\left|\mathcal{T}_D^{(0)}(\mathcal{M}_2,s_1,s_2)+\mathcal{T}_D^{(1)}(\mathcal{M}_2,s_1,s_2)\right|^2\end{aligned} \quad (36)$$

and the quantities

$$\mathcal{T}_D^{(0)}(\mathcal{M}_2,s_1,s_2) = \left\langle s_1,s_2\middle|\Psi_D^{\mathcal{M}_2}(\mathbf{k}_2)\right\rangle \quad (37)$$

and

$$\begin{aligned}\mathcal{T}_D^{(1)}(\mathcal{M}_2,s_1,s_2) &= \int\frac{d^3k_2}{2E_{\mathbf{k}_2}(2\pi)^3}\frac{f^{NN}(\boldsymbol{\kappa}_\perp)}{k_1'^2-M_N^2+i\varepsilon}\\ &\times\left\langle s_1,s_2\middle|\Psi_D^{\mathcal{M}_2}(\mathbf{p}_2)\right\rangle\end{aligned} \quad (38)$$

can be called the *reduced (Lorentz index independent) amplitudes*; in these equations $\Psi_D^{\mathcal{M}_2}$ is the deuteron wave function and the spin wave function refers to the two particles in the continuum.

In summary we have shown the following:

1. The cross section that includes FSI factorizes provided (i) the spin-flip part of the *NN* scattering amplitude can be disregarded, which is consistent with the high energies we are considering, and (ii) the momentum transfer $\boldsymbol{\kappa}$ in the *NN* rescattering is small and transverse, so that in the integral (31) one has $\mathbf{k}_2 \sim \mathbf{p}_2$ or, equivalently, $\mathbf{k}_2 \simeq \mathbf{p}_m$; this is a reasonable approximation, thanks to the behavior of the elastic *NN* scattering amplitude, which is sharply peaked in the forward direction.
2. In the eikonal approximation and neglecting the spin dependence (spin-flip part) of the *NN* amplitude, the FSI is not affected by the spin structure of the wave functions of the deuteron and the two-body final state. This means that in computing the Feynman diagrams, the intermediate spin algebra can be disregarded, and only the scalar part of the corresponding vertex functions can be considered, using Eq. (23) to define the scalar parts of the wave functions. Then the resulting amplitude has to be merely sandwiched between the spin functions of initial and final particles.

These conclusions can be generalized to a nucleus A, for which the cross section of the process $A(e,e'p)(A-1)$ is given by the following expression:

$$\frac{d^6\sigma}{dE'\,d\Omega'\,d\mathbf{p}_m} = K(Q^2,x,\mathbf{p}_m)\,\sigma^{eN}(\bar{Q}^2,\mathbf{p}_m)P_A^{\mathrm{FSI}}(\mathbf{p}_m,E_m), \quad (39)$$

where $P_A^{\mathrm{FSI}}(\mathbf{p}_m,E_m)$, the *distorted spectral function*, is given by

$$P_A^{\rm FSI}(\mathbf{p}_m, E_m) = \frac{1}{(2\pi)^3}\frac{1}{2J_A+1}\sum_f \sum_{\mathcal{M}_A,\,\mathcal{M}_{A-1},\,s_1} \times \left|\sum_{n=0}^{A-1}\mathcal{T}_A^{(n)}(\mathcal{M}_A, \mathcal{M}_{A-1}, s_1)\right|^2 \times \delta\big(E_m - \big(E_{A-1}^f + E_{\rm min}\big)\big) \quad (40)$$

and n denotes the order of rescattering. In what follows the distorted momentum distributions for the deuteron [Eq. (36)] and the distorted spectral function for ^{3}He [Eq. (40)] will be calculated within the GA and GEA.

B. The process ^{2}H$(e, e'p)n$ within the GA and GEA

Let us now calculate the reduced amplitude $\mathcal{T}_D^{(1)}$ in the process ^{2}H$(e, e'p)n$, taking FSI into account by the GEA. This amounts to replacing the energy denominator in Eq. (38) by its generalized eikonal approximation. To this end, we will consider both the "canonical" case, in which the value of the three-momenta transfers $|\mathbf{q}|$ is so high that $\mathbf{q} \simeq \mathbf{p}_1$, with the z axis naturally directed along $\mathbf{q}$, as well as the case of smaller values of $\mathbf{q}$, but high values of $\mathbf{p}_1$, when $\mathbf{q}$ and $\mathbf{p}_1$ may point in different directions, in which case the z axis is oriented along $\mathbf{p}_1$.

Remembering that $\kappa = p_1 - k_1' = k_2 - p_2$, we can write the energy denominator as follows:

$$\begin{aligned} k_1'^2 - M_N^2 &= (p_1-\kappa)^2 - M_N^2 = -2p_1\kappa + \kappa^2 \\ &= 2|\mathbf{p}_1|\left(\kappa_z + \frac{\kappa_0\big(\kappa_0 - 2E_{\mathbf{p}_1}\big)}{2|\mathbf{p}_1|} - \frac{\boldsymbol{\kappa}^2}{2|\mathbf{p}_1|}\right) \\ &\approx 2|\mathbf{p}_1|\left(\kappa_z - \frac{E_{\mathbf{k}_1+\mathbf{q}} + E_{\mathbf{p}_1}}{2|\mathbf{p}_1|}\kappa_0\right) \approx 2|\mathbf{p}_1|\,(\kappa_z + \Delta_z)\,, \end{aligned} \quad (41)$$

where

$$\Delta_z = \frac{E_{\mathbf{k}_1+\mathbf{q}} + E_{\mathbf{p}_1}}{2|\mathbf{p}_1|}(E_m - |E_A|) \quad (42)$$

and the relation

$$\kappa_0 = E_{\mathbf{p}_1} - E_{\mathbf{k}_1+\mathbf{q}} \approx -(E_m - |E_A|) \quad (43)$$

resulting from energy conservation $q_0 + M_D = E_{\mathbf{p}_1} + E_{\mathbf{p}_2}$ has been used.

By changing the normalization of the NN amplitude from the covariant one to the nonrelativistic analog ($E_{\mathbf{p}} \simeq M_N$), one has

$$\frac{f^{NN}(\boldsymbol{\kappa}_\perp)}{4E_{\mathbf{p}}|\mathbf{p}_1|} \approx \frac{f^{NN}(\boldsymbol{\kappa}_\perp)}{4M_N|\mathbf{p}_1|} = a^{\rm NR}(\boldsymbol{\kappa}_\perp) \equiv i\int d^2\mathbf{b}\, e^{i\boldsymbol{\kappa}_\perp\mathbf{b}}\,\Gamma(\mathbf{b}) \quad (44)$$

and $\mathcal{T}_D^{(1)}$ becomes

$$\mathcal{T}_D^{(1)}(\mathcal{M}_2, s_1, s_2) = \int \frac{d^3k}{(2\pi)^3} a^{NR}(\boldsymbol{\kappa}_\perp) \times \frac{1}{\kappa_z + \Delta_z + i\varepsilon}\big\langle s_1, s_2\big|\Psi_D^{\mathcal{M}_2}(\mathbf{p})\big\rangle. \quad (45)$$

Using

$$\frac{1}{\kappa_z + \Delta_z + i\epsilon} = -i\int \theta(z)\, e^{i(\kappa_z+\Delta_z)\cdot z}\, dz \quad (46)$$

we obtain, in coordinate space,

$$\mathcal{T}_D^{(0)}(\mathcal{M}_2, s_1, s_2) + \mathcal{T}_D^{(1)}(\mathcal{M}_2, s_1, s_2) = \big\langle s_1, s_2\big(1 - \theta(z)e^{i\Delta_z z}\Gamma(\mathbf{b})\big)e^{-i\mathbf{p}_m\mathbf{r}}\big|\Psi_D^{\mathcal{M}_2}(\mathbf{r})\big\rangle. \quad (47)$$

As a result, the cross section will read as follows:

$$\frac{d^6\sigma}{dE'\,d\Omega'\,d\mathbf{p}_m} = K(Q^2, x, \mathbf{p}_m)\,\sigma^{eN}(\bar{Q}^2, \mathbf{p}_m) \times n_D^{\rm FSI}(\mathbf{p}_m)\delta\big(M_D + \nu - E_{\mathbf{p}_1} - E_{\mathbf{p}_m}\big) \quad (48)$$

with the *distorted momentum distributions* $n_D^{\rm FSI}$ defined by

$$n_D^{\rm FSI}(\mathbf{p}_m) = \frac{1}{3}\frac{1}{(2\pi)^3}\sum_{\mathcal{M}_2, S_{23}}\left|\int d\mathbf{r}\,\chi_{S_{23}}^\dagger\,\Psi_D^{\mathcal{M}_2\dagger}(\mathbf{r}) \times \mathcal{S}_\Delta^{\rm FSI}(\mathbf{r})\,\exp(-i\mathbf{p}_m\mathbf{r})\right|^2, \quad (49)$$

where $S_\Delta^{\rm FSI}(\mathbf{r})$, which describes the final state interaction between the hit nucleon and the spectator, is

$$\mathcal{S}_\Delta^{\rm FSI}(\mathbf{r}) = 1 - \theta(z)e^{i\Delta_z z}\Gamma(\mathbf{b}) \quad (50)$$

with $\mathbf{r} = (\mathbf{b}, z)$. In these formulas the z axis is along $\mathbf{p}_1$; it should be pointed out, however, that at large values of the momentum transfer, the hit nucleon propagates almost along $\mathbf{q}$ so that by choosing the z axis along the three-momentum transfer and neglecting the virtuality of the struck nucleon before and after interaction, one can write [10]

$$k_1'^2 - M_N^2 = (k_1+q)^2 - M_N^2 \approx 2|\mathbf{q}|\,(\kappa_z + \Delta_z)\,, \quad (51)$$

where

$$\Delta_z = \frac{q_0}{|\mathbf{q}|}E_m. \quad (52)$$

It can be seen that the FSI factor (50) in the GEA differs from the one of the standard GA [46–48], simply by the additional factor $e^{i\Delta_z z}$. It should be pointed out that whereas the well-known factor $\theta(z)$ [47,48] originates from the nonrelativistic reduction of the covariant Feynman diagrams and guarantees the correct time ordering of the rescattering processes, the quantity Δ_z is of a pure nuclear structure origin and, as can be seen from Eq. (47), represents a correction to the parallel component of the missing momentum. Therefore the corrections from Δ_z are expected to be important in parallel kinematics at $|\mathbf{p}_z| \simeq \Delta_z$. As we shall see from the results of our calculations performed in perpendicular kinematics in the range $|\mathbf{p}_m| \leqslant 600\,{\rm MeV}/c$ and $E_m \leqslant 100\,{\rm MeV}$, one always has $|\Delta_z| \ll |\mathbf{p}|_\perp$ with $q_0/|\mathbf{q}| \simeq 1$, so that Δ_z is always very small. We can therefore anticipate that the effects of Δ_z on the experimental data we have considered are also very small.

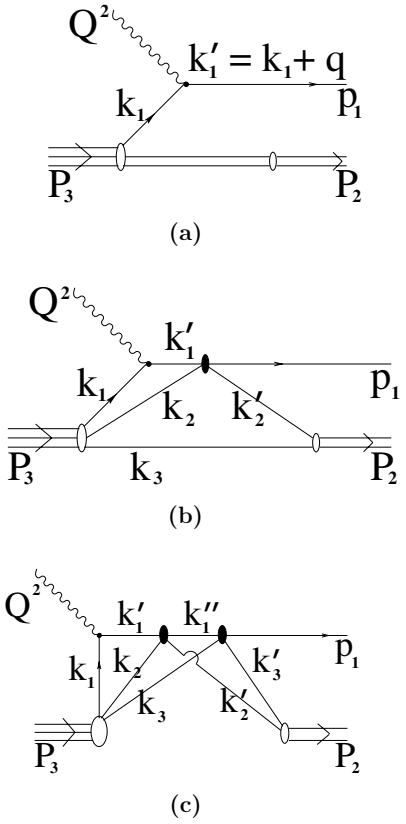

FIG. 6. Feynman diagrams representing (a) the PWIA and (b) single and (c) double rescattering in the processes ^{3}He$(e, e'p)D$ and ^{3}He$(e, e'p)(np)$. In the former case the final two-nucleon state is a deuteron with momentum $\mathbf{P}_D = \mathbf{P}_2$, whereas in the latter case the final state represents two free nucleons with momenta $\mathbf{p}_2$ and $\mathbf{p}_3$, with $\mathbf{P}_2 = \mathbf{p}_2 + \mathbf{p}_3$. The trivial single and double rescattering diagrams with nucleons "2" and "3" interchanged are not drawn. The black ovals denote the elastic NN scattering matrix $\hat{T}$ [see Eq. (25)].

C. The processes ^{3}H$(e, e'p)^2$H and ^{3}H$(e, e'p)(np)$ within the GA and GEA

Let us now consider the three-body system. The distorted spectral function is given by Eq. (40):

$$P_{\rm He}^{\rm FSI}(\mathbf{p}_m, E_m) = \frac{1}{(2\pi)^3}\frac{1}{2}\sum_f \sum_{\mathcal{M}_3, \mathcal{M}_2, s_1} \left| \sum_{n=0}^{2} \mathcal{T}_A^{(n)}(\mathcal{M}_3, \mathcal{M}_2, s_1) \right|^2 \times \delta\big(E_m - \big(E_2^f + E_{\rm min}\big)\big), \quad (53)$$

where the magnetic quantum number $\mathcal{M}_2$ refers either to the deuteron or to the "2" nucleon in the continuum, depending upon the breakup channel we are considering [$E_{\rm min} = E_3 - E_2$ ($E_{\rm min} = E_3$) for the two-body (three-body) breakup channel]. The diagrams representing the rescattering processes are shown in Fig. 6. The evaluation of these diagrams follows the standard procedure adopted for the deuteron. Let us illustrate it in the case of the 3bbu considering, for ease of presentation, the single scattering diagram of Fig. 6(b). After integration over k_{20} and k_{30} in the corresponding poles of the propagators of the spectators ($k_{20} = E_{\mathbf{k}_2}$ and $k_{30} = E_{\mathbf{k}_3}$), we obtain

$$\mathcal{T}_3^{(1)}(\mathcal{M}_3, s_1, s_2, s_3) = \int \frac{d^3k_2}{2E_{\mathbf{k}_2}(2\pi)^3}\frac{d^3k_3}{2E_{\mathbf{k}_3}(2\pi)^3} \times \frac{G_{\rm He\to 1(23)}(k_1, k_2, k_3, s_1, s_2, s_3)}{\big(k_1^2 - M_N^2\big)}\frac{f_{NN}(p_1 - k_1')}{k_1'^2 - M_N^2} \times \frac{G^+_{(23)\to f}(k_2', k_3, s_2, s_3)}{\big(k_2'^2 - M_N^2\big)}, \quad (54)$$

where the overlaps of the vertex functions G_i are

$$G_{\rm He\to 1(23)}(k_1, k_2, k_3, s_1, s_2, s_3) = \langle \mathbf{k}_1, s_1, \mathbf{k}_2, s_2, \mathbf{k}_3, s_3 | G_{\rm He\to 1(23)}(\mathcal{M}_3, \mathbf{P}_3)\rangle, \quad (55)$$

$$G_{(23)\to f}(k_2, k_3, s_2, s_3) = \big\langle \mathbf{k}_2, s_2, \mathbf{k}_3, s_3 \big| \times G_{(23)\to f}\big(\mathcal{M}_{23}, S_{23}, \mathbf{P}_2, E_2^f\big)\big\rangle. \quad (56)$$

The vertex functions G_i are replaced by the nonrelativistic overlap functions according to the general convention (where we omit for ease of presentation the proper normalization factors)

$$\big\langle s_1, s_2, s_3 \big| \Psi_{\rm He}^{\mathcal{M}_3}(\mathbf{k}_1, \mathbf{k}_2, \mathbf{k}_3)\big\rangle \approx \frac{G_{\rm He\to 1(23)}(k_1, k_2, k_3, s_1, s_2, s_3)}{\big(k_1^2 - M_N^2\big)}, \quad (57)$$

and, using the completeness relation when summing over s_2 and s_3, one gets

$$\mathcal{T}_3^{(1)}(Q^2, s_1, S_{23}) = \int \frac{d^3k_2}{2E_{\mathbf{k}_2}(2\pi)^3}\frac{d^3k_3}{2E_{\mathbf{k}_3}(2\pi)^3}\Psi^f_{(23)}(\mathbf{k}_3, \mathbf{k}_2'; S_{23}) \times \frac{f_{NN}(\kappa)}{\big(k_1'^2 - M_N^2 + i\epsilon\big)}\big\langle s_1 \big| \Psi_{\rm He}^{\mathcal{M}_3}(\mathbf{k}_1, \mathbf{k}_2, \mathbf{k}_3)\big\rangle. \quad (58)$$

Following the procedure adopted for the deuteron, we obtain

$$\begin{aligned}\mathcal{T}_3^{(1)}(Q^2, s_1, S_{23}) &= \int \frac{d^3\kappa}{(2\pi)^3\, 2E_{\mathbf{k}_2}}\Psi^f_{(23)}(\mathbf{k}_3, \mathbf{k}_2'; S_{23}) \times \frac{f_{NN}(\kappa)}{k_1'^2 - M_N^2 + i\varepsilon}\big\langle s_1 \big| \Psi_{\rm He}^{\mathcal{M}_3}(\mathbf{k}_1, \mathbf{k}_2, \mathbf{k}_3)\big\rangle \\ &\approx \int \frac{d^3\kappa}{(2\pi)^3}\Psi^f_{(23)}(\mathbf{k}_3, \mathbf{k}_2'; S_{23}) \times \frac{f_{NN}(\kappa)/4M_N|\mathbf{p}_1|}{(\kappa_z + \Delta_z + i\epsilon)} \times \big\langle s_1 \big| \Psi_{\rm He}^{\mathcal{M}_3}(\mathbf{k}_1, \mathbf{k}_2, \mathbf{k}_3)\big\rangle, \end{aligned} \quad (59)$$

where

$$\Delta_z = \frac{E_{\mathbf{k}_1+\mathbf{q}} + E_{\mathbf{p}_1}}{2|\mathbf{p}_1|}(E_m - E_3). \quad (60)$$

Including also the 2buu channel, we can write, in coordinate space,

$$P_{\rm He}^{\rm FSI}(\mathbf{p}_m, E_m) = P_{\rm gr}^{\rm FSI}(\mathbf{p}_m, E_m) + P_{\rm ex}^{\rm FSI}(\mathbf{p}_m, E_m), \quad (61)$$

where

$$P_{\rm gr}^{\rm FSI}(\mathbf{p}_m, E_m) = n_{\rm gr}^{\rm FSI}(\mathbf{p}_m)\delta(E_m - (E_3 - E_2)) \tag{62}$$

with

$$n_{\rm gr}^{\rm FSI}(\mathbf{p}_m) = \frac{1}{(2\pi)^3}\frac{1}{2}\sum_{\mathcal{M}_3,\mathcal{M}_2,s_1}\left|\int e^{i\boldsymbol{\rho}\mathbf{p}_m}\chi^{\dagger}_{\frac{1}{2}s_1}\Psi_D^{\mathcal{M}_2\,\dagger}(\mathbf{r}) \times \mathcal{S}_{\Delta}^{\rm FSI}(\boldsymbol{\rho},\mathbf{r})\Psi_{\rm He}^{\mathcal{M}_3}(\boldsymbol{\rho},\mathbf{r})\,d\boldsymbol{\rho}\,d\mathbf{r}\right|^2 \tag{63}$$

and

$$P_{\rm ex}^{\rm FSI}(\mathbf{p}_m, E_m) = \frac{1}{(2\pi)^3}\frac{1}{2}\sum_{\mathcal{M}_3,S_{23},s_1}\int\frac{d^3\mathbf{t}}{(2\pi)^3}\left|\int e^{i\boldsymbol{\rho}\mathbf{p}_m}\chi^{\dagger}_{\frac{1}{2}s_1} \times \Psi_{np}^{\mathbf{t}\dagger}(\mathbf{r})\mathcal{S}_{\Delta}^{\rm FSI}(\boldsymbol{\rho},\mathbf{r})\Psi_{\rm He}^{\mathcal{M}_3}(\boldsymbol{\rho},\mathbf{r})\,d\boldsymbol{\rho}\,d\mathbf{r}\right|^2 \times \delta\left(E_m - \frac{\mathbf{t}^2}{M_N} - E_3\right). \tag{64}$$

The FSI factor $\mathcal{S}_{\Delta}^{\rm FSI}$ describes the single and double rescattering of nucleon "1" with spectators "2" and "3" and has the following form:

$$\mathcal{S}_{\Delta}^{\rm FSI}(\boldsymbol{\rho},\mathbf{r}) = \mathcal{S}_{(1)}^{\rm FSI}(\boldsymbol{\rho},\mathbf{r}) + \mathcal{S}_{(2)}^{\rm FSI}(\boldsymbol{\rho},\mathbf{r}) \tag{65}$$

with the single-scattering contribution $\mathcal{S}_{(1)}^{\rm FSI}$ given by

$$\mathcal{S}_{(1)}^{\rm FSI}(\boldsymbol{\rho},\mathbf{r}) = 1 - \sum_{i=2}^{3}\theta(z_i - z_1)e^{i\Delta_z(z_i - z_1)}\Gamma(\mathbf{b}_1 - \mathbf{b}_i) \tag{66}$$

and the double-scattering contribution given by [10,12]

$$\mathcal{S}_{(2)}^{\rm FSI}(\boldsymbol{\rho},\mathbf{r}) = [\theta(z_2 - z_1)\theta(z_3 - z_2)\,e^{-i\Delta_3(z_2 - z_1)} \times e^{-i(\Delta_3 - \Delta_z)(z_3 - z_1)} + \theta(z_3 - z_1)\theta(z_2 - z_3)\,e^{-i\Delta_2(z_3 - z_1)} \times e^{-i(\Delta_2 - \Delta_z)(z_2 - z_1)}] \times \Gamma(\mathbf{b}_1 - \mathbf{b}_2)\Gamma(\mathbf{b}_1 - \mathbf{b}_3), \tag{67}$$

where $\Delta_i = (q_0/|\mathbf{q}|)(E_{\mathbf{p}_i} - E_{\mathbf{k}_i'})$ and Δ_z is given by Eq. (52).

When $\Delta_z = 0$, the familiar form for $\mathcal{S}^{\rm FSI}$ is obtained, namely,

$$\mathcal{S}^{\rm FSI}(\boldsymbol{\rho},\mathbf{r}) = \prod_{i=2}^{3}\left[1 - \theta(z_i - z_1)\,\Gamma(\mathbf{b}_i - \mathbf{b}_1)\right], \tag{68}$$

and when $\Gamma = 0$, the distorted spectral function (61) transforms into the usual spectral function (9).

Using Eq. (61), the cross section of the process ^{3}He$(e, e'p)X$ [$X = D$ or (np)] assumes the following form:

$$\frac{d^6\sigma}{dE'\,d\Omega'\,d\mathbf{p}_m} = K(Q^2, x, \mathbf{p}_m)\,\sigma^{eN}(\bar{Q}^2, \mathbf{p}_m)P_{\rm He}^{\rm FSI}(\mathbf{p}_m, E_m). \tag{69}$$

V. RESULTS OF THE CALCULATIONS

We have used Eqs. (48), (50), (69), and (67) to calculate the cross sections of the processes ^{2}He$(e, e'p)n$, ^{3}He$(e, e'p)^2$H, and ^{3}He$(e, e'p)(np)$. All calculations have been performed using the following well-known parametrization of the profile function $\Gamma(\mathbf{b})$:

$$\Gamma(\mathbf{b}) = \frac{\sigma_{NN}^{\rm tot}(1 - i\alpha_{NN})}{4\pi b_0^2}e^{-\mathbf{b}^2/2b_0^2}, \tag{70}$$

where $\sigma_{NN}^{\rm tot}$ is the total NN cross section, α_{NN} is the ratio of the real to imaginary part of the forward NN amplitude, and b_0 is the slope of the differential elastic NN cross section. The values of the energy-dependent quantities $\sigma_{NN}^{\rm tot}$ and α_{NN} have been taken from Ref. [49]. For the electron-nucleon cross section $\sigma^{eN}(\bar{Q}^2, \mathbf{p}_m)$ we used the De Forest $\sigma_{\rm cc1}^{eN}(\bar{Q}^2, \mathbf{p}_m)$ cross section [35]. All two- and three-body wave functions are direct solutions of the nonrelativistic Schrödinger equation; therefore our calculations are fully parameter free.

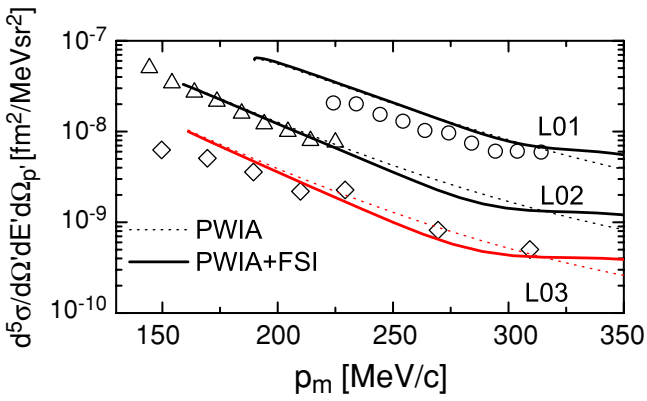

FIG. 7. (Color online) The process ^{2}H$(e, e'p)n$: The NIKHEF experimental data [17] vs the missing momentum $p_m \equiv |\mathbf{p}_m|$ are compared with our theoretical calculations; the dotted line represents the PWIA, whereas the full line includes the final state rescattering. The curves labeled L01, L02, and L03 correspond to $Q^2 = 0.1$, 0.2, and 0.3 $(\mathrm{GeV}/c)^2$, respectively, and $x \simeq 0.3$–0.6. (In this figure and in Figs. 8–12, $p' \equiv |\mathbf{p}_1|$.)

Calculations have been performed in PWIA and include the full rescattering within the GA and GEA by evaluating the Feynman diagrams shown in Figs. 5 and 6. It should be pointed out that, apart from minor differences (e.g., the structure of Δ_z for complex nuclei) that do not affect the numerical results, our GEA is essentially the same as the one developed in [10,12].

A. The process ^{2}H$(e, e'p)n$

Our results for the process ^{2}H$(e, e'p)n$ are compared in Figs. 7, 8, and 9 with three different sets of experimental data, covering different kinematical ranges, namely, the experimental data from NIKHEF [17], SLAC [19], and Jlab [18]. The relevant kinematical variables in the three experiments are as follows: (i) $0.1 \leqslant Q^2 \leqslant 0.3$, $0.3 \leqslant x \leqslant 0.6$ [17]; (ii) $1.2 \leqslant Q^2 \leqslant 6.8$, $x \simeq 1$ [19]; and (iii) $Q^2 \simeq 0.665\,(\mathrm{GeV}/c)^2$, $|\mathbf{q}| \simeq 0.7\,\mathrm{GeV}/c$, $x \simeq 0.96$ [18]. In Figs. 7 and 9 the theoretical cross section corresponding to Eq. (48), namely,

$$\frac{d^5\sigma}{dE'\,d\Omega'\,d\Omega_{\mathbf{p}_m}} = f_{\rm rec}\,\mathcal{K}(Q^2, x, \mathbf{p}_m)\,\sigma_{\rm cc1}^{eN}(\bar{Q}^2, \mathbf{p}_m)n_D^{\rm FSI}(\mathbf{p}_m), \tag{71}$$

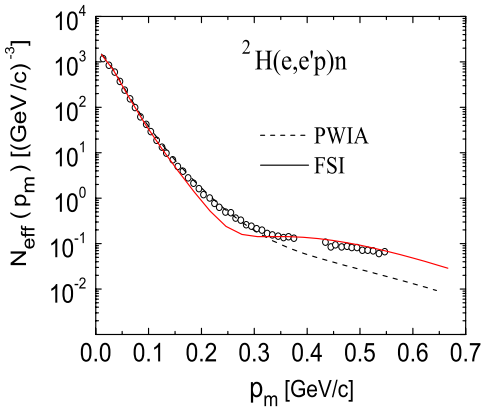

FIG. 8. (Color online) The process ^{2}H$(e, e'p)n$: The Jlab experimental data [18] [$N_{\rm eff}$ defined by Eq. (72)] vs the missing momentum $p_m \equiv |\mathbf{p}_m|$, compared with our theoretical calculations. The dotted line represents the PWIA, whereas the full line includes the final state rescattering. The experimental data correspond to the perpendicular kinematics, with $Q^2 \simeq 0.665\,(\mathrm{GeV}/c)^2$, $|\mathbf{q}| \simeq 0.7\,\mathrm{GeV}/c$, and $x \simeq 0.96$.

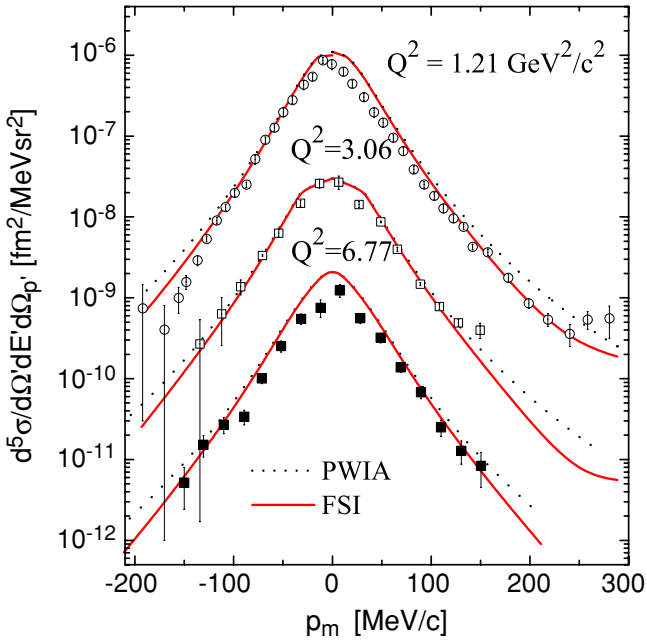

FIG. 9. (Color online) The process ^{2}H$(e, e'p)n$: SLAC experimental data at $x \simeq 1$ [19] vs the missing momentum $p_m \equiv |\mathbf{p}_m|$, compared with our theoretical calculations. The dotted lines represent the PWIA, and the full lines include the final state rescattering. The positive and negative values of p_m correspond to values of the azimuthal angle ϕ of π and 0, respectively.

is compared with the corresponding data, whereas in Fig. 8 we compare, as in Ref. [18], the effective momentum distributions $N_{\rm eff}(p_m)$ (or reduced cross section) defined by [18],

$$N_{\rm eff}(|\mathbf{p}_m|) = \frac{d^5\sigma^{\rm exp}}{d\Omega'\, dE'\, d\Omega_{\mathbf{p}_m}} \left[f_{\rm rec}\, \mathcal{K}\, \sigma^{eN}_{\rm cc1} \right]^{-1}, \qquad (72)$$

where in Eqs. (71) and (72) $f_{\rm rec}$ and $\mathcal{K}$ are kinematical factors that arise from the integration over $dT_{\mathbf{p}_1}$.

The results presented in Figs. 7–9 exhibit a general satisfactory agreement between theoretical calculations and experimental data, particularly in view of the wide range of kinematics covered by the data we have considered. Figures 8 and 9 show, however, that quantitative disagreements with data exist in some regions. Particularly worth noting is the disagreement in the region around $|\mathbf{p}_m| \simeq 0.25\,\mathrm{GeV}/c$ appearing in Fig. 8. We did not try to remove such a disagreement by adjusting the quantities entering the profile function (48), but it turns out that $n_D^{\rm FSI}$ in the region around $|\mathbf{p}_m| \simeq 0.25\,\mathrm{GeV}/c$ is rather sensitive to the value of α_{NN}. The NIKHEF kinematics deserves a particular comment. The four-momentum transfer in this experiment is rather low, raising doubts as to the validity of the eikonal approximation. In this respect, it should, however, be pointed out, that what really matters in GA and GEA is the relative three-momentum of the hit nucleon with respect to the $A-1$ system; in the NIKHEF experiment, because of the large value of the energy transfer, the three-momentum transfer is also large, and γ^* absorption occurs on a proton moving along $\mathbf{q}$, with the recoiling neutron moving with low momentum against $\mathbf{q}$; the resulting proton-neutron relative momentum is of the order of few hundred MeV$/c$, which, though representing the lower limit for the validity of the eikonal approximation, still appears, according to our results, to be suitable for the application of the GEA. In fact our results appear to be in reasonable agreement with the ones obtained within approaches that are better justified at low energies, such as, for example, the ones presented in Refs. [50–54].

Let us conclude this section by stressing that the effects of MEC and Δ-isobar excitations have been found to be very small ($\simeq$5–6%) in the SLAC kinematics (see [19]), with the results from [55] exhibiting the same trend also in the Jlab kinematics. We should also remark that the results of the GA and GEA differ by only few percent and cannot be distinguished in the figures.

B. The processes ^{3}He$(e, e'p)^2$H and ^{3}He$(e, e'p)(np)$

Calculations for the three-body systems are very involved, mainly because of the complex structure of the wave function of Ref. [2], which is given in a mixed $(L_\rho, X, j_{23}, S_{23})$ representation, including angular momentum values up to $L_\rho = 7$ and $j_{23} = 8$ [a total of 58 configurations with different combinations of $(L_\rho, X, j_{23}, S_{23})$ quantum numbers]. Correspondingly, the wave function of the spectators (the deuteron or the continuum two-nucleon states) is given in a JLS scheme (see Appendix A). We would like to stress that no approximations have been made in the evaluation of the single- and double-scattering contributions to the FSI: Proper intrinsic coordinates have been used and the energy dependence of the profile function has been taken into account in the properly chosen c.m. system of the interacting pair. The Feynman diagrams that have to be evaluated for both the 2bbu and 3bbu channels are shown in Fig. 6.

1. *The two-body breakup channel* ^{3}He$(e, e'p)^2$H

The 2bbu channel cross section

$$\frac{d^5\sigma}{dE'\,d\Omega'\,d\Omega_{\mathbf{p}_1}} = K_{2\mathrm{bbu}}(Q^2, x, \mathbf{p}_m)\,\sigma_{\mathrm{cc1}}^{eN}(\bar{Q}^2, \mathbf{p}_m)\,n_{\mathrm{gr}}^{\mathrm{FSI}}(\mathbf{p}_m) \tag{73}$$

obtained from Eq. (69), with $n_{\mathrm{gr}}^{\mathrm{FSI}}(\mathbf{p}_m)$ given by Eq. (63), is compared in Fig. 10 with recent experimental data from the Jlab collaboration [21]. The relevant kinematical variables in the experiment are $|\mathbf{q}| = 1.5\,\mathrm{GeV}/c$, $q_0 = 0.84\,\mathrm{GeV}$, $Q^2 = 1.55\,(\mathrm{GeV}/c)^2$, and $x \approx 1$. The cross section is presented as a function of the missing momentum $|\mathbf{p}_m|$ (which, for the ^{3}He$(e, e'p)D$ process, exactly coincides with the final deuteron momentum). In PWIA the cross section is directly proportional to n_{gr} [Eq. (11)], shown in the left panel of Fig. 3. It can be seen that, up to $|\mathbf{p}_m| \sim 400\,\mathrm{MeV}/c$, the PWIA and FSI results are almost the same and agree fairly well with the experimental data, which means, in turn, that the 2bbu ^{3}He$(e, e'p)^2$H does provide information on n_{gr}; in contrast, at larger values of $|\mathbf{p}_m| \geqslant 400\,\mathrm{MeV}/c$ the PWIA appreciably underestimates the experimental data. It is very gratifying to see that when FSI is taken into account, the disagreement is fully removed and an overall very good agreement between theoretical predictions and experimental data is obtained. It should be pointed out that the experimental data shown in Fig. 10 correspond to the perpendicular kinematics, when the deuteron momentum (the missing momentum) is always almost perpendicular to the momentum transfer $\mathbf{q}$; such kinematics maximize the effects from FSI, whereas in the so-called parallel kinematics, the effects are minimized (see, e.g., [9], [48], [56]). The kinematics therefore reflects itself in the relevance of the calculated FSI; in fact, we have found that the effects of the FSI calculated within either the GA or GEA approximations, differ by only a few percent, which was expected in view of the observation that the factor Δ_z [Eq. (60) or (52)] affects only the longitudinal component of $\mathbf{p}_m$ and therefore has minor effects on the data we have considered. The effects of MEC and Δ-isobar contributions have been estimated in [55] and were found to be negligible up to about $p_m \simeq 600\,\mathrm{MeV}/c$.

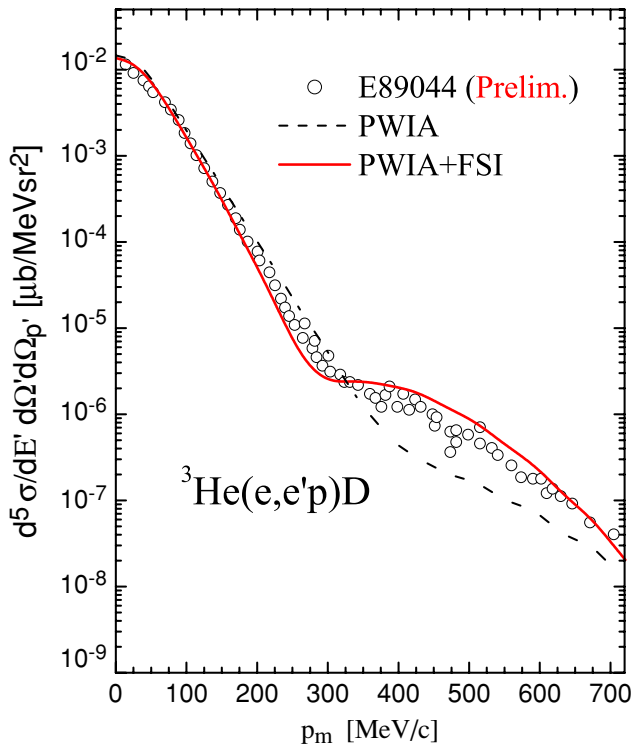

FIG. 10. (Color online) The process ^{3}He$(e, e'p)D$: Experimental data from JLab (JLab Experiment E-89-044 [21]) vs $p_m \equiv |\mathbf{p}_m|$ compared, at $Q^2 = 1.55\,(\mathrm{GeV}/c)^2$ and $x = 1$, with our theoretical results. The dashed line corresponds to the PWIA, and the full line includes the full FSI calculated using Eq. (63); the predictions by Eq. (65) (GEA) and Eq. (68) (GA) differ by at most 4% and cannot be distinguished in the figure (three-body wave function from [2]; AV18 interaction from [5]).

2. *The three-body breakup channel* ^{3}He$(e, e'p)(np)$

From Eq. (69), we obtain the cross section for the 3bbu in the following form:

$$\frac{d^6\sigma}{dE'\,d\Omega'\,d\Omega_{\mathbf{p}_1}dE_m} = K_{3\mathrm{bbu}}(Q^2, x, \mathbf{p}_m) \times \sigma_{\mathrm{cc1}}^{eN}(\bar{Q}^2, \mathbf{p}_m)\,P_{\mathrm{ex}}^{\mathrm{FSI}}(\mathbf{p}_m, E_m), \tag{74}$$

where $P_{\mathrm{ex}}^{\mathrm{FSI}}(\mathbf{p}_m, E_m)$ is given by Eq. (64). We have calculated Eq. (74) correspondending to two different kinematical ranges: the one from Ref. [20] and the one corresponding to the experimental data from Jlab [22]. In contrast to the results from the 2bbu channel, the 3bbu cross section depends on an extra kinematical variable, the removal energy E_m, and corresponds to the process in which three particles interact in the continuum. We have considered three different theoretical approaches:

1. the PWA, when FSI effects are completely ignored, that is, the three particles in the continuum are described by plane waves;
2. the PWIA, in which the struck nucleon is described in the continuum by a plane wave and the spectator pair is described by the continuum solution of the Schrödinger equation (obviously, in the case of the deuteron the PWIA coincides with the PWA); and
3. the full FSI, when the struck nucleon interacts in the continuum with the nucleons of the spectator pair via the standard GA or the more refined GEA.

In Fig. 11 the results of our calculations are compared with the experimental data from Ref. [20]. In the experiment, which corresponds to a relatively low beam energy ($E = 0.560$ GeV), the scattering angle ($\theta_e = 25^\circ$) and the energy transfer ($q_0 = 0.32$ GeV) were kept constant, and protons with different values of the missing momentum and energy were detected correspondending to several values of the proton emission angle $\theta_{\mathbf{p}_1}$: $\theta_{\mathbf{p}_1} = 45^\circ$, 60°, 90.5°, 112°, and 142.5°. The kinematics is far from the quasi-elastic peak ($x \simeq 0.1$) and the values of the four- and three-momentum transfers are low [$Q^2 \simeq 0.03\,(\mathrm{GeV}/c)^2$ and $|\mathbf{q}| = 0.28\,\mathrm{GeV}/c$]. At first glance this would invalidate the use of the eikonal approximation; however, a detailed analysis of the kinematics shows that the

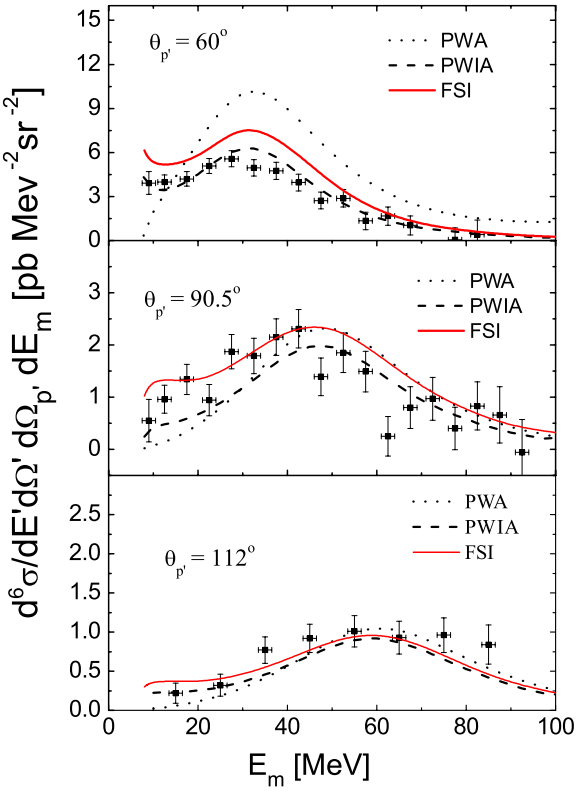

FIG. 11. (Color online) The process ^{3}He$(e, e'p)(np)$: Experimental data from Saclay [20] vs E_m and for various values of the proton emission angle $\theta_{\mathbf{p}_1}$ ($p' \equiv |\mathbf{p}_1|$) are compared with our theoretical results. The dotted lines correspond to the PWA, when the three nucleons in the final state are described by plane waves; the dashed lines correspond to the PWIA, when the interaction in the spectator neutron-proton pair is taken into account; and the full lines include the full FSI calculated using Eq. (63); the predictions by Eq. (65) (GEA) and Eq. (68) (GA) differ by at most 4% and cannot be distinguished in the figure. Note that the values of the experimental p_m and E_m corresponding to the maxima of the cross section satisfy to a large extent the relation predicted by the two-nucleon correlation mechanism [38], namely, $E_m \simeq p_m^2/4M_N$ (cf. Fig. 3, right panel), with the full FSI mainly affecting only the magnitude of the cross section (three-body wave function from [2]; AV18 interaction from [5]).

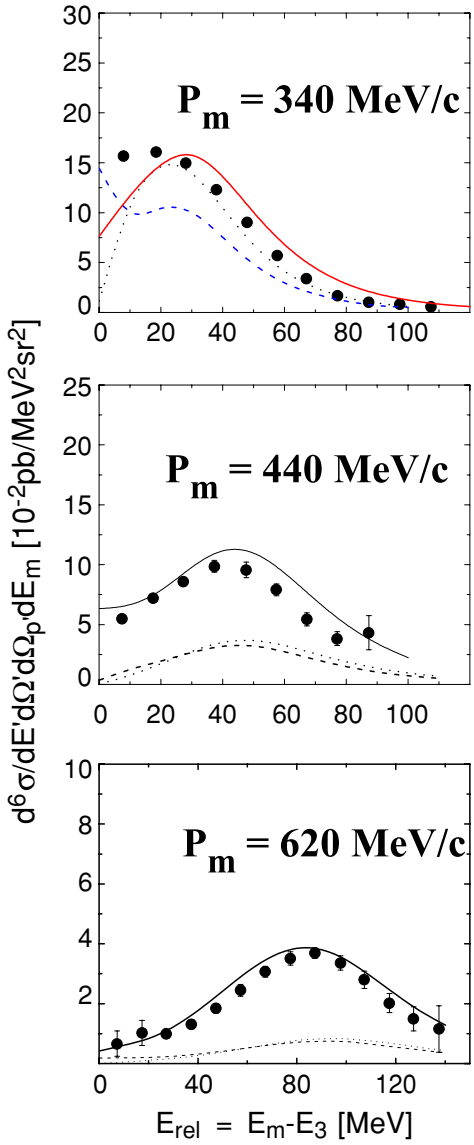

FIG. 12. (Color online) The process ^{3}He$(e, e'p)(np)$: Same as in Fig. 11 but for the Jlab experimental data [22] at $Q^2 = 1.55\,(\mathrm{GeV}/c)^2$ and $x = 1$. Note that, unlike what is shown in Fig. 11, here the differential cross section is plotted vs the excitation energy of the two-nucleon system in the continuum, i.e., $E_{\mathrm{rel}} = \mathbf{t}^2/M_N = E_2^f = E_m - E_3$.

value of both $\mathbf{p}_1$ and $\mathbf{p}_m$ are rather large (400–600 MeV/c), and so is the value of the angle between them ($\theta_{\widehat{\mathbf{p}_1\mathbf{p}_m}} \sim 150^\circ$); thus the momentum of the struck nucleon relative to the spectator pair is high enough to justify use of the eikonal approximation. Moreover, the values of the experimentally measured missing momenta and missing energy at each value of $\theta_{\mathbf{p}_1}$ always cover the kinematical range where the condition for a two-nucleon correlation mechanism $E_m \sim \mathbf{p}_m^2/4M_N$ holds; in fact, as can be seen from Fig. 11, the positions of the bumps in the cross section are reasonably predicted by the PWA and PWIA.

The results presented in Fig. 11 clearly show that, with increasing missing momentum, the experimental peak moves to higher values of missing energy, in qualitative agreement with the two-nucleon correlation mechanism. More important, it can be seen that at the highest value of $|\mathbf{p}_m|$ ($\theta_{\mathbf{p}_1} = 112^\circ$) the effects of FSI, both in the spectator pair and between the struck nucleon and the spectator pair, is very small. The reason for such a behavior is that the kinematics of the experiment is not purely perpendicular: The relation between $|\mathbf{p}_{m\perp}|$ and $|\mathbf{p}_m|$ is such that $|\mathbf{p}_{m\perp}| \sim \frac{1}{2}|\mathbf{p}_m|$, so that the dominant role played by FSI in the purely perpendicular kinematics diminishes with increased values of $\theta_{\mathbf{p}_1}$.

In Fig. 12 our results are compared with the recent data from Jlab [22], where the cross section was measured at fixed values $|\mathbf{p}_m|$ versus the missing energy E_m. As in the case of the Saclay data previously analyzed, even in this case the cross section exhibits bumps approximately located at values of E_m and $|\mathbf{p}_m|$ satisfying the two-nucleon correlation mechanism relation ($E_m \sim \mathbf{p}_m^2/4M_N$), and in agreement with the behavior

of the spectral function (see Figs. 3 and 4). However, in contrast to the Saclay case, the PWIA dramatically underestimates the experimental data. This is clear evidence that the FSI between the struck nucleon and the nucleons of the spectator pair [Feynman diagrams in Fig. 6(b) and Fig. 6(c)] does play a relevant role, as the results of our calculations (the full line in Fig. 12) do indeed really show. Since, as already stressed, the Jlab experiment corresponds to perpendicular kinematics, this explains the larger effects of the FSI with respect to the Saclay experiment. The effects of the FSI calculated within either the GA or GEA approximations differ only by a few percent, which was expected in view of the observation that the factor Δ_z [Eq. (60) or (52)] affects only the longitudinal component of $\mathbf{p}_m$ and therefore has minor effects on the data we have considered.

There exist at present only two approaches to the calculations of the 2bbu and 3bbu channels at the Jlab kinematics: the one presented in this paper and the one by Laget reported in Refs. [21–23]. A comparison of the results of the two approaches exhibits an encouraging agreement in both the 2bbu and 3bbu channels, with some minor differences that should most likely be ascribed to the different wave functions used in the two calculations. It is therefore gratifying to observe that different approximations to the treatment of FSI lead to very similar results.

The effects of MEC and Δ, as previously pointed out, have not yet been considered in our approach; the calculation of Ref. [23] shows they reduce the cross section in the peak by about 10%, leaving the missing energy dependence and, consequently, our conclusions, practically unchanged.

VI. SUMMARY AND CONCLUSIONS

We have calculated the cross section of the processes ^{2}H$(e, e'p)n$, ^{3}He$(e, e'p)D$, and ^{3}He$(e, e'p)(np)$, using realistic wave functions for the ground state, which exhibits the very rich correlation structure generated by modern *NN* interactions; the FSI of the struck nucleon with the spectators have been treated within the standard Glauber eikonal approximation [16], as well as with its generalized version (GEA) [9–11]. The two approaches differ by a factor Δ_z [Eqs. (42) and (52)], which modifies [see Eq. (65)] the FSI factor appearing in the standard GA [Eq. (68)]. This factor takes into account the removal energy of the struck nucleon in the *NN* scattering amplitude, or, equivalently, the excitation energy of the system $A-1$. By properly choosing the z axis (along $\mathbf{q}$ or $\mathbf{p}_1$), we were able to calculate FSI effects for large values of the three-momentum transfer $\mathbf{q}$ or for large values of the momentum of the struck nucleon $\mathbf{p}_1$ relative to the $A-1$ system; by this method calculations could be extended successfully even at relatively low values of Q^2. For the three-body breakup channel in ^{3}He, the FSI in the spectator pair was always calculated by the solution of the Schrödinger equation, whereas the interaction of the active, fast nucleon with the two nucleons of the spectator pair has been taken care of by the GA or GEA approximations. The method we have used is a very transparent one and fully parameter free: It is based on Eqs. (49), (61), and (65), which only require knowledge of the nuclear wave functions, since the FSI factor is fixed directly by *NN* scattering data. Of course, with increasing A, the order of rescattering increases up to the $(A-1)$-th order; we have performed calculations in the three-body case exactly but did not investigate the problem of the convergence of the multiple scattering series. This problem is under investigation for ^{4}He. Most of our calculations have been performed in kinematical conditions where the effects of MEC, Δ-isobar creation, etc., are minimized, as confirmed by calculations performed, for example, in Refs. [23,50–53,55,57,58]. The main results we have obtained are as follows:

1. The agreement between the results of our calculations and the experimental data for both the deuteron and ^{3}He is a very satisfactory one, particularly in view of the lack of any adjustable parameter in our approach.
2. The effects of the FSI are such that they systematically bring theoretical calculations in better agreement with the experimental data. For some quantities, FSI simply improve the agreement between theory and experiment (cf., e.g., Figs. 7, 9, and 11), whereas for some other quantities, they play a dominant role (see, e.g., Figs. 10 and 12).
3. A comparison of the PWA and the PWIA with the full FSI calculation does show that proper kinematics conditions could be found corresponding to an overall very small effect of FSI, thus leaving room for the investigation of details of the nuclear wave function; in fact, we always found that in the 3bbu channel in ^{3}He, ^{3}He$(e, e'p)(np)$, the experimental values of p_m and E_m corresponding to the maximum values of the cross section satisfy to a large extent the relation predicted by the two-nucleon correlation mechanism [38], namely, $E_m \simeq p_m^2/4M_N + E_3$ (cf. Fig. 3, right panel), with the full FSI mainly affecting only the magnitude of the cross section; thus, quasi-elastic one-nucleon emission $A(e, e'p)B$ processes at $x \simeq 1$, together with processes at $x \simeq 2$, when the virtual photon is absorbed by a correlated two-nucleon "system," would represent a valuable tool for the investigation of correlations in nuclei.
4. Calculations of the 2bbu channel disintegration of ^{4}He, that is, the process ^{4}He$(e, e'p)^3$H, have already been performed [15] using realistic wave functions and taking exactly into account nucleon rescattering up to third order, that is, by using the generalization of Eq. (65) to the four-particle case,
$$\mathcal{S}_\Delta^{\rm FSI} = \mathcal{S}_{(1)}^{\rm FSI}(\mathbf{R}, \mathbf{r}_{12}, \mathbf{r}_{34}) + \mathcal{S}_{(2)}^{\rm FSI}(\mathbf{R}, \mathbf{r}_{12}, \mathbf{r}_{34}) + \mathcal{S}_{(3)}^{\rm FSI}(\mathbf{R}, \mathbf{r}_{12}, \mathbf{r}_{34}), \quad (75)$$
where $\mathbf{R}$, $\mathbf{r}_{12}$, and $\mathbf{r}_{34}$ are four-body Jacobi coordinates. Calculations for the 3bbu and 4bbu channels are in progress and will be reported elsewhere [59]; they should in principle yield results appreciably differing from the predictions based on shell-model-type four-body wave functions.
5. Our results for ^{3}He generally agree with the ones obtained in Ref. [23], so that it would appear that the problem of the treatment of FSI at high values of Q^2 (or high $\mathbf{p}_1$) is under control; nevertheless, a systematic comparison of the various approaches would be highly desirable.
6. We have given the criteria according to which at high energies the exclusive $A(e, e'p)B$ cross section should factorize, and the similarity of our results with the ones

based on a nonfactorized cross section [23] confirm the validity of these criteria.

7. In the kinematical range we have considered, only minor numerical differences were found between the conventional Glauber eikonal approach and its generalized extension; this does not mean that the same will hold in other kinematical conditions (see, e.g., [9–11]).

ACKNOWLEDGMENTS

The authors are indebted to A. Kievsky for making available the variational three-body wave functions of the Pisa Group and to G. Salmè for useful discussions about their use. Thanks are due to M. A. Braun and D. Treleani for stimulating discussions on the Feynman diagram approach to nucleon rescattering. Many useful discussions with various members of the Jlab Experiment E-89-044 are gratefully acknowledged. We express our gratitude to M. Alvioli for a careful reading of the manuscript. L.P.K. is indebted to the University of Perugia and INFN, Sezione di Perugia, for a grant and for warm hospitality. This work was partially supported by the Italian Ministero dell'Istruzione, Università e Ricerca (MIUR), through the funds COFIN01, and by the Russian Fund for Basic Research 00-15-96737.

APPENDIX A: THE NUCLEAR WAVE FUNCTIONS

In our calculations we have used two- and three-body wave functions corresponding to the AV18 potential [5].

1. The ground-state wave function of ^{3}He

For the ^{3}He wave function we have adopted the correlated variational wave function by the Pisa group [2], which is written in a mixed $(L_\rho, X, j_{23}, S_{23})$ representation, where j_{23} and S_{23} are the total angular momentum and the total spin of the pair "23," X is an intermediate angular momentum resulting from the coupling $\mathbf{j}_{23} + \mathbf{s}_1$, and L_ρ is the radial angular momentum of the motion of the nucleon "1" relative to the pair "23." The explicit form of the wave function is

$$\begin{aligned}\Psi_{\rm He}^{\mathcal{M}_3}(\boldsymbol{\rho}, \mathbf{r}) &= \sum_{\{\alpha\}} \sum_{\{m\}} \left\langle X M_X\, L_\rho m_\rho \middle| \frac{1}{2} \mathcal{M}_3 \right\rangle \left\langle j_{23} m_{23}\, \frac{1}{2} \sigma_1 \middle| X M_X \right\rangle \\ &\times \chi_{\frac{1}{2}\sigma_1} \mathrm{Y}_{L_\rho M_\rho}(\hat{\boldsymbol{\rho}})\, \langle l_{23} \mu_{23}\, S_{23} \nu_{23} | j_{23} m_{23} \rangle \\ &\times Y_{l_{23}\mu_{23}}(\hat{\mathbf{r}}) \chi_{S_{23}\nu_{23}} R_{\{\alpha\}}(r, \rho)\, \mathcal{I}^{T_{23}}_{\frac{1}{2}\frac{1}{2}}, \end{aligned} \tag{A1}$$

where $\{\alpha\}$ labels all possible configurations in ^{3}He with quantum numbers L_ρ, X, j_{23}, S_{23}, and T_{23} and $\langle l_1 m_1 l_2 m_2 | l_{12} m_{12} \rangle$ is a Clebsch-Gordan coefficient. The total isospin function is $\mathcal{I}^{T_{23}}_{\frac{1}{2}\frac{1}{2}} = \sum \langle T_{23} \tau_{23} \frac{1}{2} \tau_1 | \frac{1}{2} \frac{1}{2} \rangle \mathcal{J}_{T_{23}\tau_{23}} \eta_{\frac{1}{2}\tau_1}$, where $\mathcal{J}_{T_{23}\tau_{23}}$ and $\eta_{\frac{1}{2}\tau_1}$ are the isospin functions of the pair and the nucleon, respectively. Obviously, because of Pauli principle and parity constraints, the allowed configurations in Eq. (A1) are those that satisfy the following conditions:

$$L_\rho + l_{23} \text{ is even}, \qquad \text{and} \qquad l_{23} + S_{23} + T_{23} \text{ is odd}. \tag{A2}$$

The corresponding radial part of the wave function, $R_{\{\alpha\}}(r, \rho)$, has been obtained [2] by a variational method using the AV18 potential including values of $L_\rho, l_{12} = 0, \ldots, 9$ (for a total of 58 different configurations of L_ρ, X, j_{23}, l_{23}, S_{23}) in the calculations.

2. The two-body continuum wave function $\Psi^{\mathbf{t}}_{23}(\mathbf{r})$

With the representation (A1) of the ^{3}He wave function, it was convenient to adopt for the two-nucleon scattering state $\Psi^{\mathbf{t}}_{23}(\mathbf{r})$ the spin-channel representation $\Psi^{\mathbf{t}}_{S_{23}\nu_{23}}(\mathbf{r})$, characterized by the total (conserved in the scattering process) spin S_{23} and its projection ν_{23}. For spin $S_{23} = 1$ one has

$$\begin{aligned}\Psi^{\mathbf{t}}_{S_f \nu_f}(\mathbf{r}) = 4\pi \sum_{J_f M_f} \sum_{l_0 l_f} &\langle l_0 \mu_0\, S_f \nu_f | J_f M_f \rangle \\ &\times \mathrm{Y}_{l_0\mu_0}(\hat{\mathbf{t}}) R^{|\mathbf{t}|}_{J_f, l_0 l_f}(r) i^{l_f} \mathcal{Y}^{J_f M_f}_{1 l_f}(\hat{\mathbf{r}}) \mathcal{J}_{T_{23}\tau_{23}}, \end{aligned} \tag{A3}$$

where $l_0, l_f = J_f \pm 1, J_f$. Note that the presence of tensor forces in the NN potential leads to an admixture of partial waves with $l = J_f - 1$ and $l = J_f + 1$. This hinders the use of real phase shifts for the asymptotic behavior of the radial functions $R^{|\mathbf{t}|}_{J_f, l_0 l_f}(r)$ and, consequently, the Schrödinger equation cannot be solved in terms of real solutions. However, a unitary transformation V allows one to define new radial functions $\tilde{R} = VR$ that are eigenfunctions of the scattering problem, that is, solutions of the Schrödinger equation with the proper asymptotic behavior.

3. Wave function overlaps and the spectral function $P(|\mathbf{k}_1|, E)$ of ^{3}He

The spectral function for the three-body breakup channel can be expressed in terms of the overlap between the three-body and two-body radial functions by substituting (A1)–(A3) into Eq. (12). Using the orthogonality of the spherical harmonics $\mathrm{Y}_{lm}(\hat{\mathbf{t}})$ and the completeness of the Clebsch-Gordan coefficients, one obtains that only diagonal ($\{\alpha\} = \{\alpha_N\}$) matrix elements contribute to the spectral function, namely,

$$\begin{aligned} P_{\rm ex}(|\mathbf{k}_1|, E) &= \frac{1}{2} \sum_{\mathcal{M}_3} \sum_{\sigma_f, S_f, \nu_f} \int \frac{d^3\mathbf{t}}{(2\pi)^3} \left| \int d\boldsymbol{\rho}\, d\mathbf{r}\, \Psi^{\mathcal{M}_3}_{\rm He}(\boldsymbol{\rho}, \mathbf{r}) \right. \\ &\left. \times \Psi^{\mathbf{t}}_{S_f \nu_f}(\mathbf{r}) e^{-i\boldsymbol{\rho}\mathbf{k}_1} \right|^2 \delta\left(E_m - \frac{\mathbf{t}^2}{M_N} - E_3 \right) \\ &= \frac{M_N \sqrt{M_N E_{\rm rel}}}{2\pi^3} f_{\rm iso} \sum_{\{\alpha\}} \left| \int \rho^2\, d\rho\, j_{L_\rho}(p\rho) \mathcal{O}^{E_{\rm rel}}_{\{\alpha\}}(\rho) \right|^2, \end{aligned} \tag{A4}$$

where $f_{\rm iso} = 3(1)$ for the pair in the isosinglet (isotriplet) final state, $j_{L_\rho}(p\rho)$ are the spherical Bessel functions, and the dimensionless overlap integrals $\mathcal{O}^{E_{\rm rel}}_{\{\alpha\}}(\rho)$ are defined as

follows:

$$\mathcal{O}^{E_{\rm rel}}_{\{\alpha\}}(\rho) = \int R_{\{\alpha\}}(r,\rho)\tilde{R}^{|\mathbf{t}|}_{\{\alpha\}}(r) r^2\, dr. \tag{A5}$$

The normalization of the proton spectral function (A4)–(A5) is

$$\int d^3\mathbf{k}_1\, dE\, P(|\mathbf{k}_1|, E) \approx \begin{cases} 0.15 \text{ for } T_{23}=0 \\ 0.50 \text{ for } T_{23}=1 \end{cases} \tag{A6}$$

so that the two-body breakup channel is normalized to $\approx$1.35. Since the FSI factors $S^{\rm FSI}$ and $S^{\rm FSI}_{\Delta}$ [Eqs. (65) and (68)] are not spherically symmetric, the distorted spectral function $P^{\rm FSI}_{\rm ex}(\mathbf{p}_m, E_m)$ [Eq. (64)] is no longer diagonal with respect to the $(L_\rho, X, j_{23}, S_{23})$ configurations. Except for parity constraints (A2), any values of angular momenta of the pair in the final state contribute to $P^{\rm FSI}_{\rm ex}(\mathbf{p}_m, E_m)$.

APPENDIX B: FACTORIZATION OF THE COVARIANT CROSS SECTION

In this appendix we will show, within a fully covariant approach, that under certain kinematical conditions the cross section for the $A(e,e'p)X$ process factorizes even in the presence of FSI. We shall consider, to this end, the deuteron treated within the Bethe-Salpeter (BS) formalism. As mentioned, the factorization depends on the spin structure of the square of the matrix element $[\bar{u}(\mathbf{k}_1,\tilde{s}_1)\Phi_D^{\mathcal{M}_2}(k_1,k_2)(\hat{k}_2+M_N)v(\mathbf{k}_2,s_2)]$ appearing in Eq. (19) or, in case of FSI, on the structure of $[\bar{u}(\mathbf{k}_1,\tilde{s}_1)\Phi_D^{\mathcal{M}_2}(k_1,k_2)v(\mathbf{k}_2,s_2)]$ [cf. Eq. (28)]. The relevant spin parts can be evaluated directly by using the explicit form of the Dirac spinors, u and v, and the explicit expressions for the amplitudes $\Phi_D^{\mathcal{M}_2}(k_1,k_2)$ (cf. Refs. [42,43,45]).

1. The PWIA

In Ref. [44] the Feynman diagrams for the process $D(e,e'p)X$ have been evaluated including all BS components. Here we recalculate the diagrams for the $^3S_1^{++}$ and $^3D_1^{++}$ components in a slightly different manner that will be useful when FSI effects are considered.

In PWIA the cross section reads as follows:

$$\frac{d^5\sigma}{dE'\,d\Omega'} = \sigma_{\rm Mott}\tilde{l}^{\mu\nu}L^D_{\mu\nu}\frac{d^3p_1}{(2\pi)^3 2E_1}\frac{d^3p_2}{(2\pi)^3 2E_2}, \tag{B1}$$

where $\tilde{l}^{\mu\nu}$ and $L^D_{\mu\nu}$ are the leptonic and hadronic tensors, respectively, the latter being

$$\begin{aligned} L^D_{\mu\nu} &= \frac{1}{2M_D}\frac{1}{3}\sum_{\mathcal{M}_2,s_1,s_2} T_\mu(\mathcal{M}_2,s_1,s_2)T_\nu(\mathcal{M}_2,s_1,s_2)(2\pi)^3\delta^{(4)} \\ &\quad\times(P_D+q-p_1-p_2) \\ &= \frac{1}{2M_D}\frac{1}{3}\sum_{\mathcal{M}_2,s_1,s_2}\langle\mathcal{M}_2|\hat{J}^N_\mu|p_2,s_2,p_1,s_1\rangle\langle p_1,s_1,p_2,s_2 \\ &\quad\times|\hat{J}^N_\nu|\mathcal{M}_2\rangle(2\pi)^3\delta^{(4)}(P_D+q-p_1-p_2), \end{aligned} \tag{B2}$$

where $\hat{J}^N_\mu$ is the nucleon electromagnetic current operator. The amplitude T_μ could be written in the following form:

$$\begin{aligned} T_\mu(\mathcal{M}_2,s_1,s_2) &= \bar{u}(\mathbf{p}_1,s_1)\Gamma^{\gamma^*N}_\mu\left(Q^2,k_1^2\right) \\ &\quad\times\Phi_D^{\mathcal{M}_2}(k_1,k_2)\tilde{S}^{-1}(\hat{k}_2)v(\mathbf{p}_2,s_2), \end{aligned} \tag{B3}$$

where $\Phi_D^{\mathcal{M}_2}$ is a shorthand notation for the main BS amplitudes $\Phi_{^3S_1^{++}}$ and $\Phi_{^3D_1^{++}}$, corresponding to $L=0$ and $L=2$, respectively (see Refs. [42,45]), $k_2=p_2$, $\hat{S}^{-1}(\hat{k}_2)=\hat{k}_2+m$, and $\Gamma^{\gamma^*N}_\mu(Q^2,k_1^2)$ is the electromagnetic eN vertex, which, for an off-mass-shell nucleon, depends not only on Q^2 but on $k_1^2\neq m^2$ as well.

By introducing between $\Gamma_\mu(Q^2,p_1,k_1)$ and $\Phi_D^{\mathcal{M}_D}(k_1,k_2)$ the complete set of the Dirac spinors

$$\frac{1}{2M_N}\sum_{\tilde{s}_1}[u(\mathbf{k}_1,\tilde{s}_1)\bar{u}(\mathbf{k}_1,\tilde{s}_1)-v(\mathbf{k}_1,\tilde{s}_1)\bar{v}(\mathbf{k}_1,\tilde{s}_1)] \tag{B4}$$

and bearing in mind that for the $^3S_1^{++}$ and $^3D_1^{++}$ partial waves the second term in (B4) does not contribute, we obtain

$$\begin{aligned} T_\mu(\mathcal{M}_2,s_1,s_2) &= \frac{1}{2M_N}\sum_{\tilde{s}_1}J^{eN}_\mu(Q^2,p_1,k_1,\tilde{s}_1,s_1) \\ &\quad\times\left[\bar{u}(\mathbf{k}_1,\tilde{s}_1)\Phi_D^M(k_1,k_2)\tilde{S}^{-1}(\hat{k}_2)v(\mathbf{p}_2,s_2)\right], \end{aligned} \tag{B5}$$

where $J^{eN}_\mu(Q^2,p_1,k_1)=\langle\mathbf{p}_1,s_1|\Gamma^{\gamma^*N}_\mu(Q^2,k_1^2)|\mathbf{k}_1,\tilde{s}_1\rangle$.

Evaluating Eq. (B5) for the D wave, we have

$$\begin{aligned} &\left[\bar{u}(\mathbf{k}_1,\tilde{s}_1)\Phi^{\mathcal{M}_2}_{^3D_1^{++}}(k_1,k_2)\tilde{S}^{-1}(\hat{k}_2)v(\mathbf{p}_2,s_2)\right] \\ &= -\frac{NN_1^2}{\sqrt{2}}\left(k_2^2-M_N^2\right)\phi_D(k_0,|\mathbf{k}|)\,2m\langle\chi^\dagger_{\tilde{s}_1}|\{-(\boldsymbol{\sigma}\boldsymbol{\xi}^M) \\ &\quad+3(\mathbf{n}\boldsymbol{\xi}^M)(\mathbf{n}\boldsymbol{\sigma})\}|\widetilde{\chi}_{s_2}\rangle, \end{aligned} \tag{B6}$$

where $\mathbf{n}$ is a unit vector along $\mathbf{k}$, that is, $\mathbf{n}=\mathbf{k}/|\mathbf{k}|=\mathbf{k}_1/|\mathbf{k}_1|$. When Eq. (B6) is inserted in the expression for the cross section, we obtain

$$\begin{aligned} &\frac{1}{3}\sum_{\mathcal{M}_2,s_2}\left\langle\chi_{\tilde{s}_1}\right|\{-(\boldsymbol{\sigma}\boldsymbol{\xi}^{\mathcal{M}_2})+3(\mathbf{n}\boldsymbol{\xi}^{\mathcal{M}_2})(\mathbf{n}\boldsymbol{\sigma})\}\left|\widetilde{\chi}_{s_2}\right\rangle\left\langle\widetilde{\chi}_{s_2}\right| \\ &\quad\times\{-(\boldsymbol{\sigma}\boldsymbol{\xi}^{+\mathcal{M}_2})+3(\mathbf{n}\boldsymbol{\xi}^{+}M)(\mathbf{n}\boldsymbol{\sigma})\}\left|\chi_{\tilde{s}_1}\right\rangle=2\delta_{\tilde{s}_1\tilde{s}'_1}. \end{aligned} \tag{B7}$$

The last relation ensures factorization of the cross section; in fact, by performing the same procedure for the S wave, it easy to show that, because of Eq. (B7), the cross section [Eq. (B1)] factorizes, assuming the form (24) with n_D given by Eq. (22). In obtaining these equations we expressed the BS amplitudes $\phi_L(k_0,|\mathbf{k}|)$ in terms of the BS vertices $G_{^3L_1^{++}}(k_0,|\mathbf{k}|)$ and the radial functions u_L, by the relations

$$\frac{NN_1^2}{\sqrt{2}}\left(k_2^2-M_N^2\right)\phi_D(k_0,|\mathbf{k}|)=\frac{NN_1^2 2E_{\mathbf{k}}}{\sqrt{2}}\frac{G_{^3D_1^{++}}(k_0,|\mathbf{k}|)}{M_D-2E_{\mathbf{k}}}, \tag{B8}$$

where $k_0=M_D/2-E_{\mathbf{k}}$, and

$$u_{S(D)}=\frac{G_{^3S_1^{++}(^3D_1^{++})}(k_0,|\mathbf{k}|)/(4\pi)}{\sqrt{2M_D}(M_D-2E_{\mathbf{k}})}. \tag{B9}$$

Note that in Eq. (B9) the normalization of the wave function is chosen so as to correspond to the nonrelativistic deuteron

wave function

$$\frac{2}{\pi}\int |\mathbf{k}|^2 d|\mathbf{k}|\left(u_S^2(|\mathbf{k}|)+u_D^2(|\mathbf{k}|)\right)\approx 1. \tag{B10}$$

We reiterate that factorization in PWIA occurs because the sum over s_2 and $\mathcal{M}_2$ of the square of the matrix element in Eq. (B7) becomes diagonal with respect to $\tilde{s}_1$.

When FSI are taken into account, instead of Eq. (B7), one obtains for the D wave

$$\begin{aligned}
&\frac{1}{3}\sum_{\mathcal{M}_2,s_2}\left[\bar{u}(\mathbf{k}_1,s_1)\Phi_D^{\mathcal{M}_2}(k_1,k_2)v(\mathbf{k}_2,s_2)\right]^\dagger\\
&\quad\times\left[\bar{u}(\mathbf{k}_1',\tilde{s}_1)\Phi_D^{\mathcal{M}_2}(k_1',k_2')v(\mathbf{k}_2',s_2)\right]\\
&\quad\times\frac{1}{3}\sum_{M,s_2}\left\langle\chi_{s_1}\middle|\{-(\boldsymbol{\sigma}\boldsymbol{\xi}^{\mathcal{M}_2})+3(\mathbf{n}\boldsymbol{\xi}^{\mathcal{M}_2})(\mathbf{n}\boldsymbol{\sigma})\}\middle|\widetilde{\chi}_{s_2}\right\rangle\\
&\quad\times\left\langle\widetilde{\chi}_{s_2}\middle|\{-(\boldsymbol{\sigma}\boldsymbol{\xi}^{+\mathcal{M}_2})+3(\mathbf{n}'\boldsymbol{\xi}^{+\mathcal{M}_2})(\mathbf{n}'\boldsymbol{\sigma})\}\middle|\chi_{\tilde{s}_1}\right\rangle\\
&=\frac{1}{3}\sum_{\mathcal{M}_2}\left\langle\chi_{s_1}\middle|\{-(\boldsymbol{\sigma}\boldsymbol{\xi}^{\mathcal{M}_2})+3(\mathbf{n}\boldsymbol{\xi}^{\mathcal{M}_2})(\mathbf{n}\boldsymbol{\sigma})\}\right.\\
&\quad\left.\times\{-(\boldsymbol{\sigma}\boldsymbol{\xi}^{+\mathcal{M}_2})+3(\mathbf{n}'\boldsymbol{\xi}^{+\mathcal{M}_2})(\mathbf{n}'\boldsymbol{\sigma})\}\middle|\chi_{\tilde{s}_1}\right\rangle,
\end{aligned}\tag{B11}$$

where $\mathbf{n}(\mathbf{n}')$ is a unit vector along $\mathbf{k}_1(\mathbf{k}_2')$. (For the S wave the spin structure is trivial.)

By taking into account the completeness of the polarization vectors $\boldsymbol{\xi}$, the only spin dependence remaining in Eq. (B11) is contained in the term

$$\frac{1}{3}\sum_M(\mathbf{n}\boldsymbol{\xi}^M)(\mathbf{n}\boldsymbol{\sigma})(\mathbf{n}'\boldsymbol{\xi}^{+M})(\mathbf{n}'\boldsymbol{\sigma})=(\mathbf{n}\mathbf{n}')((\mathbf{n}\mathbf{n}')-i\boldsymbol{\sigma}[\mathbf{n}\times\mathbf{n}']), \tag{B12}$$

so that for rescattering with low momentum transfer, in the integral over $\mathbf{k}_2$ the main contribution comes from $\mathbf{k}_2\sim\mathbf{p}_2$, $\mathbf{k}_2'\sim\mathbf{p}_2$, and one has $\boldsymbol{\sigma}[\mathbf{n}\times\mathbf{n}']=0$ and factorization is approximately recovered, with the S and D waves adding incoherently.

Thus, in summary, factorization is compatible with FSI if the following conditions hold:

1. The spin-flip part of the NN amplitude should be very small, as it occurs when either the three-momentum transfer $\mathbf{q}$ or the momentum $|\mathbf{p}_1|$ is large.
2. The momentum transfer $\boldsymbol{\kappa}$ in the NN rescattering has to be small so that, in the integral, $\mathbf{k}_2\sim\mathbf{p}_2$. This appears to be the case since the NN amplitude is sharply peaked forward.
3. The contribution from $N\bar{N}$ pair currents can be neglected, which is to a large extent legitimate owing to the smallness of the P wave in the deuteron.

[1] W. Glöckle, H. Witala, D. Huber, H. Kamada, and J. Golak, Phys. Rep. **274**, 107 (1996).
[2] A. Kievsky, S. Rosati, and M. Viviani, Nucl. Phys. **A551**, 241 (1993); A. Kievsky (private communication).
[3] S. C. Pieper and R. B. Wiringa, Ann. Rev. Nucl. Part. Sci. **51**, 53 (2001).
[4] S. C. Pieper, R. B. Wiringa, and V. R. Pandharipande, Phys. Rev. C **46**, 1741 (2000).
[5] R. B. Wiringa, V. G. J. Stoks, and R. Schiavilla, Phys. Rev. C **51**, 38 (1995).
[6] V. N. Gribov, Sov. Phys. JETP **30**, 709 (1970).
[7] L. Bertocchi, Nuovo Cimento A **11**, 45 (1972).
[8] J. H. Weis, Acta Phys. Pol. B **7**, 851 (1976).
[9] L. L. Frankfurt, W. R. Greenberg, G. A. Miller, M. M. Sargsian, and M. I. Strikman, Z. Phys. A **352**, 97 (1995).
[10] L. L. Frankfurt, M. M. Sargsian, and M. I. Strikman, Phys. Rev. C **56**, 1124 (1997).
[11] M. M. Sargsian, Int. J. Mod. Phys. E **10**, 405 (2001).
[12] M. M. Sargsian, T. V. Abrahamyan, M. I. Strikman, and L. L. Frankfurt, arxiv: nucl-th/0406020.
[13] M. A. Braun, C. Ciofi degli Atti, and D. Treleani, Phys. Rev. C **62**, 034606 (2000).
[14] M. Braun, C. Ciofi degli Atti, L. P. Kaptari, Eur. J. Phys. A **19**, 143 (2004).
[15] H. Morita, M. Braun, C. Ciofi degli Atti, and D. Treleani, Nucl. Phys. **A699**, 328c (2002).
[16] R. J. Glauber, in *Lectures in Theoretical Physics*, Vol. I, p. 315, edited by W. E. Brittin and L. G. Dunham (Wiley Interscience, New York, 1959).
[17] W.-J. Kasdorp *et al*., Few-Body Syst. **25**, 115 (1998).
[18] P. E. Ulmer *et al*., Phys. Rev. Lett. **89**, 062301 (2002).
[19] H. J. Bulten *et al*., Phys. Rev. Lett. **74**, 4775 (1995).
[20] C. Marchand *et al*., Phys. Rev. Lett. **60**, 1703 (1988).
[21] M. M. Rvachev *et al*., arxiv: nucl-ex/0409005v2.
[22] F. Benmokhtar *et al*., arxiv: nucl-ex/0408015v2.
[23] J.-M. Laget, arxiv: nucl-th/0410003.
[24] J. J. van Leeuwe *et al*., Phys. Lett. **B523**, 6 (2001).
[25] S. Janssen, J. Ryckebusch, W. Van Nespen, and D. Debruyne, Nucl. Phys. **A672**, 285 (2000).
[26] C. Ciofi degli Atti and L. P. Kaptari, in *International Workshop on Probing Nucleons and Nuclei via the* $(e,e'p)$ *Reaction*, Eds. D. Higinbotham, J. M. Laget, and E. Voutier (The Print House, New York 2004), p. 121.
[27] M. Alvioli, C. Ciofi degli Atti, L. P. Kaptari, and H. Morita, *Proceedings of the 6th Workshop on Electromagnetically Induced Two Hadron Emission*, Pavia, Italy, 24–27 Sept. 2003.
[28] S. Boffi, C. Giusti, and F. D. Pacati, Phys. Rep. **226**, 1 (1993).
[29] R.-W. Schulze and P. E. Sauer, Phys. Rev. C **226**, 38 (1993).
[30] C. Ciofi degli Atti, E. Pace, and G. Salmè, Phys. Rev. C **21**, 805 (1980).
[31] A. Kievski, E. Pace, G. Salmè, and M. Viviani, Phys. Rev. C **56**, 64 (1997).
[32] C. Ciofi degli Atti, E. Pace, and G. Salmè, in *Lecture Notes in Physics* (Springer, Berlin, 1978), Vol. 86, p. 315.
[33] H. Meier-Hajduk, Ch. Hajduk, P. E. Sauer, and W. Theis, Nucl. Phys. **A395**, 332 (1983); U. Oelfke, P. U. Sauer, and F. Coester, *ibid.* **A518**, 593 (1990).
[34] C. Ciofi degli Atti, L. Kaptari, and S. Scopetta, Eur. Phys. J. A **5**, 191 (1999).
[35] T. de Forest, Jr., Nucl. Phys. **A392**, 232 (1983).
[36] R.V. Reid, Jr., Ann. Phys. **50**, 411 (1968).

[37] L. L. Frankfurt and M. I. Strikman, Phys. Rep. **160**, 235 (1988).
[38] C. Ciofi degli Atti, S. Simula, L. L. Frankfurt, and M. I. Strikman, Phys. Rev. C **44**, R7 (1991); C. Ciofi degli Atti and S. Simula, *ibid.* **53**, 1689 (1996).
[39] J. Golak, H. Witala, R. Skininski, W. Glöckle, A. Nogga, and H. Kamada, Phys. Rev. C **70**, 034005 (2004).
[40] C. Ciofi degli Atti and L. P. Kaptari, Phys. Rev. C **66**, 044004 (2002).
[41] S. Jeschonnek, Phys. Rev. C **63**, 034609 (2001); J. Ryckebusch *et al*., Nucl. Phys. **A728**, 226 (2003).
[42] B. D. Keister and J. A. Tjon, Phys. Rev. C **26**, 578 (1982); G. Rupp and J. A. Tjon, *ibid*. **41**, 472 (1990); J. J. Kubis, Phys. Rev. D **6**, 547 (1972); M. J. Zuilhof and J. A. Tjon, Phys. Rev. C **22**, 2369 (1980).
[43] F. Gross, Phys. Rev. **186**, 1448 (1969); W. W. Buck and F. Gross, Phys. Rev. C **20**, 2361 (1979); F. Gross, J. V. Van Orden, and K. Holinde, *ibid*. **45**, 2094 (1992).
[44] C. Ciofi degli Atti, D. Faralli, A. Yu. Umnikov, and L. P. Kaptari, Phys. Rev. C **60**, 034003 (1999).
[45] L. P. Kaptari, B. Kampfer, S. M. Dorkin, and S. S. Semikh, Few Body Syst. **27**, 189 (1999); Phys. Rev. C **57**, 1097 (1998).
[46] C. Ciofi degli Atti, L. P. Kaptari, and D. Treleani, Phys. Rev. C **63**, 044601 (2001).
[47] N. N. Nikolaev, J. Speth, and B. G. Zakharov, JETP **82**, 1046 (1996).
[48] A. Bianconi, S. Jeschonnek, N. N. Nikolaev, and B. G. Zacharov, Phys. Lett. **B343**, 13 (1995).
[49] R. A. Arndt *et al*., "Partial-Wave Analysis Facility (SAID)", http://said.phys.vt.edu/.
[50] J.-M. Laget, Phys. Lett. **B199**, 1046 (1987).
[51] F. Ritz, H. Göller, T. Wilbois, and H. Arenhövel, Phys. Rev. C **55**, 2214 (1997).
[52] G. Beck and H. Arenhövel, Few-Body Syst. **13**, 165 (1992).
[53] G. Beck, T. Wilbois, and H. Arenhövel, Few-Body Syst. **17**, 91 (1994).
[54] E. Hummel and J. A. Tjon, Phys. Rev. C **49**, 21 (1994).
[55] J.-M. Laget, Few-Body Syst. Suppl. **15**, 171 (2003).
[56] H. Morita, C. Ciofi degli Atti, and D. Treleani, Phys. Rev. C **60**, 34603 (1999).
[57] J.-M. Laget, Phys. Rev. D **579**, 333 (1994).
[58] J.-M. Laget, in *New Vistas in Electronuclear Physics*, edited by E. Tomusiak *et al*. (Plenum, New York, 1986), p. 361.
[59] M. Alvioli, C. Ciofi degli Atti, L. Kaptari, and H. Morita (in preparation).